Contrasting impacts of humidity on the ozonolysis of monoterpenes: insights into the multi-generation chemical mechanism

Shan Zhang, Lin Du*, Zhaomin Yang, Narcisse Tsona Tchinda, Jianlong Li, Kun Li*

Environment Research Institute, Shandong University, Qingdao 266237, China.

Correspondence to: Lin Du (lindu@sdu.edu.cn) and Kun Li (kun.li@sdu.edu.cn)

Abstract. Secondary organic aerosol (SOA) formed from the ozonolysis of biogenic monoterpenes is a major source of atmospheric organic aerosol. It has been previously found that relative humidity (RH) can influence the SOA formation from some monoterpenes, yet most studies only observed the increase or decrease in SOA yield without further explanations of molecular-level mechanisms. In this study, we chose two structurally different monoterpenes (limonene with an endocyclic double bond and an exocyclic double bond, Δ^3-carene with only an endocyclic double bond) to investigate the effect of RH in a set of oxidation flow reactor experiments. We find contrasting impacts of RH on the SOA formation: limonene SOA yield increases by ~100% as RH increases, while there is a slight decrease in Δ^3-carene SOA yield. Although the complex processes in the particle phase may play a role, we primarily attribute it to the water-influenced reactions after ozone attack on the exocyclic double bond of limonene, which leads to the increment of lower volatile organic compounds under high RH condition. However, as Δ^3-carene only has an endocyclic double bond, it cannot undergo such reactions. This hypothesis is further supported by the SOA yield enhancement of β-caryophyllene, a sesquiterpene that also has an exocyclic double bond. These results greatly improve our understanding of how water vapor influences the ozonolysis of biogenic organic compounds and subsequent SOA formation processes.

1 Introduction

Secondary organic aerosol (SOA), as an important type of ambient fine particulate matter (PM$_{2.5}$: aerosols with aerodynamic diameter $\leq$ 2.5 μm) (Guo et al., 2014; Huang et al., 2014), has caused a series of negative impacts on human health (Pye et al., 2021), air quality (Zhang et al., 2016) and global climate (Levy et al., 2013). SOA produced from the oxidation of biogenic volatile organic compounds (BVOCs) is a major component of SOA in heavy forest regions during summer (Sindelarova et al., 2014; Ahmadov et al., 2012), and contributes by a large fraction (~40%-80%) to global OA budget (Cholakian et al.,

2019).

Monoterpenes, mostly emitted from coniferous trees, account for ~11% in total BVOCs (Sindelarova et al., 2014; Kanakidou et al., 2005). Limonene is one of the most abundant monoterpenes, with the annual emission budget of 11.4 Tg yr^{-1} (Guenther et al., 2012). Apart from the biogenic source, limonene can also be released from the indoor emission, mainly from essential oils (Ravichandran et al., 2018; De Matos et al., 2019; Mot et al., 2022). Limonene has an endocyclic double bond and an exocyclic double bond, and is thus more reactive than other monoterpenes towards oxidants such as ozone (O_3), hydroxyl radical (OH), and nitrate radical (NO_3) (Chen and Hopke, 2010; Atkinson and Arey, 2003). Δ^3-carene is another kind of monoterpene that dominates the monoterpene emission from Scots pine (Bäck et al., 2012). Different from limonene, Δ^3-carene contains only one endocyclic double bond, which is similar to most other monoterpenes.

Ozonolysis is an important reaction pathway for limonene and Δ^3-carene. Although reactions with OH and NO_3 are faster than that with O_3 for both two monoterpenes (Atkinson, 1991; Khamaganov and Hites, 2001; Chen et al., 2015; Shaw et al., 2018), the atmospheric concentration of the latter monoterpene is much higher than that of the former (Sbai and Farida, 2019). The contributions of O_3-reactions with limonene and Δ^3-carene to tropospheric degradation are 47% and 24%, respectively, in the daytime (Ziemann and Atkinson, 2012). In pristine areas where NO_3 concentration is very low, ozonolysis is also the dominant fate for limonene and Δ^3-carene in the nighttime. In addition, it has been previously found that the ozonolysis of monoterpenes can produce more extremely low volatility products than OH-initiated oxidation, which contributes by a large fraction to the SOA production (Jokinen et al., 2015). For either limonene or Δ^3-carene, the first step for ozonolysis is attacking on the endocyclic double bond to form two types of stabilized Criegee intermediates (sCI) with low energy (Fig. S1) (Drozd and Donahue, 2011; Chen et al., 2019). The sCI will then trigger a series of chemical reactions, like isomerization, decomposition and addition reactions. Correspondingly, the major components in Δ^3-carene SOA are caric acid, OH-caronic acid, and caronic acid (Ma et al., 2009; Thomsen et al., 2021), while the major components from limonene SOA are limonaldehyde, keto-limonon aldehyde, limononic acid and keto-limononic acid (Pathak et al., 2012; Wang and Wang, 2021).

Water is ubiquitous in the atmosphere and can affect the formation mechanism of SOA and its relevant physical and chemical properties (Sun et al., 2013). A number of field measurements have shown

60 that the average molecular weight of the water/organic phase and activity coefficient of condensed

61 organics would be changed due to the change of relative humidity (RH) (Seinfeld et al., 2001; Li et al.,

62 2020). In addition, several laboratory studies have demonstrated that RH can influence the ozonolysis of

63 monoterpenes in different ways. Most of those studies have reported either an inhibitory effect or a

64 negligible effect of high RH on the particle formation (Bonn and Moortgat, 2002; Fick et al., 2002; Zhao

65 et al., 2021; Ye et al., 2018). Nevertheless, few other studies found that high RH can promote SOA

66 formation from the ozonolysis of limonene (Yu et al., 2011; Gong et al., 2018; Xu et al., 2021), but the

67 reason of this promotion effect remains unclear.

68   To fully examine the effects of water on SOA formation from the ozonolysis of monoterpenes,

69 especially the related chemical processes, we used an oxidation flow reactor (OFR) to investigate the

70 ozonolysis of limonene and Δ^3-carene under different RH conditions in this study. An ultra-high

71 performance liquid chromatography with a quadrupole time-of-flight mass spectrometer (UPLC-Q-TOF-

72 MS) was deployed to analyze the molecular chemical composition of the SOA, which provided insights

73 into the physical and chemical processes influenced by the water content. With these state-of-the-art

74 techniques, we proposed mechanisms that may explain the inhibitory or enhancing RH effects on SOA

75 formation for different monoterpenes.

76 **2 Experimental methods**

77 **2.1 Oxidation flow reactor experiments**

78   A series of dark ozonolysis experiments of limonene and Δ^3-carene were conducted in a custom-

79 made oxidation flow reactor (OFR). The OFR is a 602 mm long stainless cylinder with a volume of 2.5

80 L (Fig. S2) (Liu et al., 2019; Liu et al., 2014). A zero-air generator (XHZ2000B, Xianhe, China) was

81 used to generate dry clean air as the carrier gas for the OFR. As shown in Fig. S2, there are four gas paths

82 upstream of the OFR: the first path is the precursor gas channel through which monoterpenes are injected

83 via a syringe pump (ISPLab 01, Shenchen, China); the second path is for the flow of 300 sccm dry zero

84 air passing through a mercury lamp (λ = 185 nm) to generate O_3; the third path is connected to a water

85 bubbler to generate wet air; the fourth path is the extra dry zero air entering the OFR. The RH in the OFR

86 was controlled by adjusting the ratio of the wet and dry zero air flows. A water recycle system was

87 equipped to keep the temperature (T) around at 298 K. The total flow was 0.9 L min^{-1}, resulting in an

88 average residence time of 167 s. The RH and T in the OFR were monitored by a T/RH Sensor (HM40,

89 VAISALA, Finland). The concentration of ozone and the consumption of the precursor gas were

90 measured with an ozone monitor (Model 106L, 2B Technologies, USA) and a gas chromatography with

91 flame ionization detector (GC-FID 7890B, Agilent Technologies, USA), respectively. The GC was

92 equipped with a DB-624 column (30 m × 0.32 mm, 1.8 µm film thickness) whose temperature was set

93 to ramp from 100 °C to 180 °C at a rate of 20 °C min^{-1}, and then held at 180 °C for 2 min. Before each

94 experiment, O_3 was introduced into the OFR to clean it until the background aerosol mass concentration

95 reached < 1 µg m^{-3}.

96   The experimental conditions are shown in Table 1. In these OFR experiments, the precursor

97 (limonene or Δ^3-carene) concentration was set to ~320-340 ppb. A high O_3 concentration of ~6 ppm was

98 used to realize an equivalent aging time of 0.41 day in the real atmosphere, assuming an average ambient

99 O_3 concentration of 28 ppb (Sbai and Farida, 2019) (see Section S1 for the calculation). Under such

100 conditions, most of the precursors were consumed, since the residence time was almost five and three

101 times of the half-life for limonene and Δ^3-carene, respectively. Correspondingly, the O_3 consumption for

102 limonene and $\Delta3$-carene were ~250 ppb and ~100 ppb, respectively. A series of RH conditions ranging

103 from dry (1-2%) to 60% with a step of ~10% were used to investigate the effects of water content on

104 SOA production and composition (see Table 1). All materials used in the experiments have been

105 described in Section S2.

106 **Table 1.** Experimental conditions and results.

Exp.	[Precursor] (ppb)	[O]$_3$ (ppm)	T (K)	RH (%)	N$_{(13.8-723.4\ nm)}$[a] (cm^{-3})	M$_{(13.8-723.4\ nm)}$[b] (µg m^{-3})	D$_{(mean)}$[c] (nm)	SOA yield (%)
				limonene				
1	321±39	5.7	298	1–2	6.9×10^5	980.9	138.2	62.9
2	321±39	6.0	298	10±2	1.3×10^6	1377.5	126.8	88.4
3	321±39	5.9	298	20±2	9.0×10^5	1573.3	150.9	90.2
4	321±39	5.9	298	30±2	1.4×10^6	1573.3	128.9	100.9
5	321±39	6.0	298	40±2	1.7×10^6	2051.4	130. 7	131.6
6	321±39	5.5	298	50±2	1.5×10^6	1962.7	137.8	125.9

7	321±39	5.5	298	60±2	$1.5×10^6$	2211.1	139.0	141.8
				Δ^3-carene				
8	341±28	6.1	298	1–2	$9.5×10^4$	346.0	195.8	19.4
9	341±28	6.4	298	10±2	$1.4×10^5$	300.3	163.4	16.8
10	341±28	6.4	298	20±2	$9.4×10^4$	244.9	176.9	13.7
11	341±28	6.0	298	30±2	$5.9×10^4$	241.2	205.1	13.5
12	341±28	6.3	298	40±2	$4.6×10^4$	205.8	203.2	11.5
13	341±28	6.3	298	50±2	$6.8×10^4$	196.7	180.7	11.0
14	341±28	6.3	298	60±2	$5.6×10^4$	198.5	190.2	11.1

107 [a] $N_{(14.1-735\ nm)}$ means the total particle number concentration from size 13.8 nm to 723.4 nm. [b] $M_{(13.8-723.4\ nm)}$
108 means the total particle mass concentration from size13.8 nm to 723.4 nm. [c] $D_{(mean)}$ means the particle
109 mean diameter.

110 **2.2 SOA particle analysis**

111 **2.2.1 SOA yield**

112 The SOA particle size distribution was measured with a scanning mobility particle sizer (SMPS),

113 which consists of a differential mobility analyzer (DMA) (model 3082, TSI Inc., USA) and a

114 condensation particle counter (CPC) (model 3776, TSI Inc., USA). The samples were measured by SMPS

115 every 5 minutes with a sampling flow and a sheath flow of 0.3 L min^{-1} and 3 L min^{-1}, respectively. The

116 SOA mass concentration was calculated from the volume concentration measured with SMPS and the

117 aerosol density, which was estimated to be 1.25 cm^{-3} for limonene- and 1.09 g cm^{-3} for Δ^3-carene-SOA

118 (Thomsen et al., 2021; Watne et al., 2017).

119 The SOA yield (Y) for individual organic gas can be calculated as:

120
$$Y = \frac{\Delta M}{\Delta HC}$$

121 Where ΔM is the total mass concentration of SOA, ΔHC is the mass concentration of reacted precursor

122 (Ng et al., 2007; Odum et al., 1996).

123 **2.2.2 Ultra-high performance liquid chromatography quadrupole time-of-flight mass spectrometry**
124 **analysis**

125 An ultra-high performance liquid chromatography (UPLC, UltiMate 3000, Thermo Scientific)

126 coupled with a quadrupole time-of-flight mass spectrometry (Q-TOFMS, Bruker Impact HD) was used

127   to analyze the molecular-level chemical composition of SOA. First, the SOA particles were collected on

128   the PTFE filters (47 mm diameter, 0.22 μm pore size, Jinteng, China). Next, these filters were dissolved

129   and extracted by 5 mL methanol for two times. Extracts were then filtered through PTFE syringe filters

130   (0.22 μm pore size), and were concentrated to near dryness by nitrogen-blowing. At last, the samples

131   were redissolved in a 200 μL solution with 0.1% (v/v) formic acid in 50:50 methanol/ultrapure water

132   mixture.

133   The parameters of LC-MS were set as follows: capillary voltage 4000 V, nebulizer pressure 0.4 bar,

134   dry heater temperature 200℃, end plate voltage −500 V, and flow of dry gas 4 L min^{-1}. A C_{18} column

135   (100 Å, 3 mm particle size, 2.1 mm×50 mm, Waters, USA) was used with a column temperature of 35℃.

136   The mobile phase was 0.1 % formic acid in methanol (A) and 0.1 % formic acid in ultra-high purity

137   water (B) with a flow of 200 μL min^{-1}. The injection volume was 5 μL. The MS was operated in negative

138   ion mode, and the detection molecular weight range was from m/z 50 to 1500. The temperature ramp

139   program was: 0–3min with 0%–3% phase B, 3–25min with 3%–50% phase B, 25–43min with 50%–90%

140   phase B, 43–48 min with 90%–3% phase B, 48–60min with 3% phase B.

141   **3 Results and discussion**

142   **3.1 SOA production under different RH conditions**

143   SOA formation of a representative experiment is shown in Fig. S3. It is found that the formed SOA

144   are mainly in the size range of 60-200 nm, and the number concentration and mass concentration are

145   relatively stable during the course of the OFR experiment. SOA formation from limonene and Δ^3-carene

146   in terms of particle number concentration, particle mass concentration, and SOA yield as a function of

147   RH are illustrated in Fig. 1a-c. We find that all the above-mentioned 3 parameters of limonene-SOA

148   increase with the increasing RH. The increment of particle mass concentration and SOA yield from the

149   ozonolysis of limonene is ~100% higher at wet (60% RH) than at dry conditions. In contrast, SOA

150   formation from Δ^3-carene is suppressed by ~40% under high RH. The distinct effects of RH on SOA

151   formation from the ozonolysis of limonene and Δ^3-carene found in this study agree with most previous

152   studies (Yu et al., 2011; Jonsson et al., 2006b; Bonn et al., 2002; Gong and Chen, 2021; Li et al., 2019b).

153   As shown in Table 2, Yu et al. (2011) reported a positive correlation between SOA production and RH

154   for the ozonolysis of limonene in the chamber experiments without OH scavenger. Their experimental

155   condition is similar to that in our study regarding the absence of OH scavenger and, thus, similar results

156   were observed. However, in the presence of OH scavenger, results are quite different. Jonsson et al. (2006)

157   observed a similar enhancement effect of high RH on SOA production with 2-butanol as the OH

158   scavenger, while Bonn et al. (2002) found a negligible or suppressive effect with cyclohexane as the OH

159   scavenger. It should be noted that the OH scavenger not only has the ability to scavenge OH but also

160   produces additional products which may influence the reactions of target precursors. For example, there

161   is no difference between 2-butanol and cyclohexane in the scavenging ability of OH radical, though 2-

162   butanol will produce more $HO_2\cdot$ than cyclohexane and, consequently, $R\cdot$ will react with $HO_2\cdot$ to produce

163   more hydroxyl acids and hydroxyl per-acid products, most of which have low volatility and, thus high

164   partitioning into the particle phase. According to previous studies, the influence of different OH

165   scavengers can vary (Jonsson et al., 2008). This may explain the different findings with and without OH

166   scavenger for limonene-SOA. With regard to Δ^3-carene, similar results are found in the absence of OH

167   scavenger, namely, high RH has negligible or slightly suppressive effect on SOA production (Bonn et al.,

168   2002; Fick et al., 2002). Same as limonene, the presence of OH scavenger and its different chemical

169   nature can explain the different results found previously (Jonsson et al., 2006a; Bonn et al., 2002).

170   The enhancement in limonene-SOA production under high RH can be due to several reasons from

171   either physical or chemical processes. First, the hygroscopic growth of the particles (i.e., absorption of

172   water content) can lead to higher mass concentration under higher RH, but the enhancement should be

173   at most ~30% as the growth factor (GF, the ratio of wet and dry diameter: $D_{wet/Ddry}$) of limonene-SOA is

174   ≤1.1 (Varutbangkul et al., 2006). However, we do not observe an obvious change in the mean diameter

175   when comparing dry and wet conditions (Fig. 1d). In addition, hygroscopic growth should also occur for

176   Δ^3-carene SOA, but no obvious enhancement in particle mass is observed (Fig. 1a). Therefore, it is

177   suggested that physical processes regarding hygroscopic growth play a minor role in the enhancement in

178   limonene-SOA under high RH. As a consequence, we believe that chemical processes are likely the

179   reason of the enhancement in limonene-SOA under high RH. Water can influence chemical processes in

180   the gas phase or in the particle phase. Particle-phase reactions can promote the growth of small particles

181   and, thus, mainly lead to larger particle sizes. As the observed SOA enhancement is mainly from high

182   number concentration particles rather than the large size particles (Fig. 1b and 1d), it is likely that the

183   water-participated gas-phase reactions are the most possible reasons for the limonene-SOA enhancement.

184   The reaction mechanism is analyzed below based on the mass spectra information on the SOA.
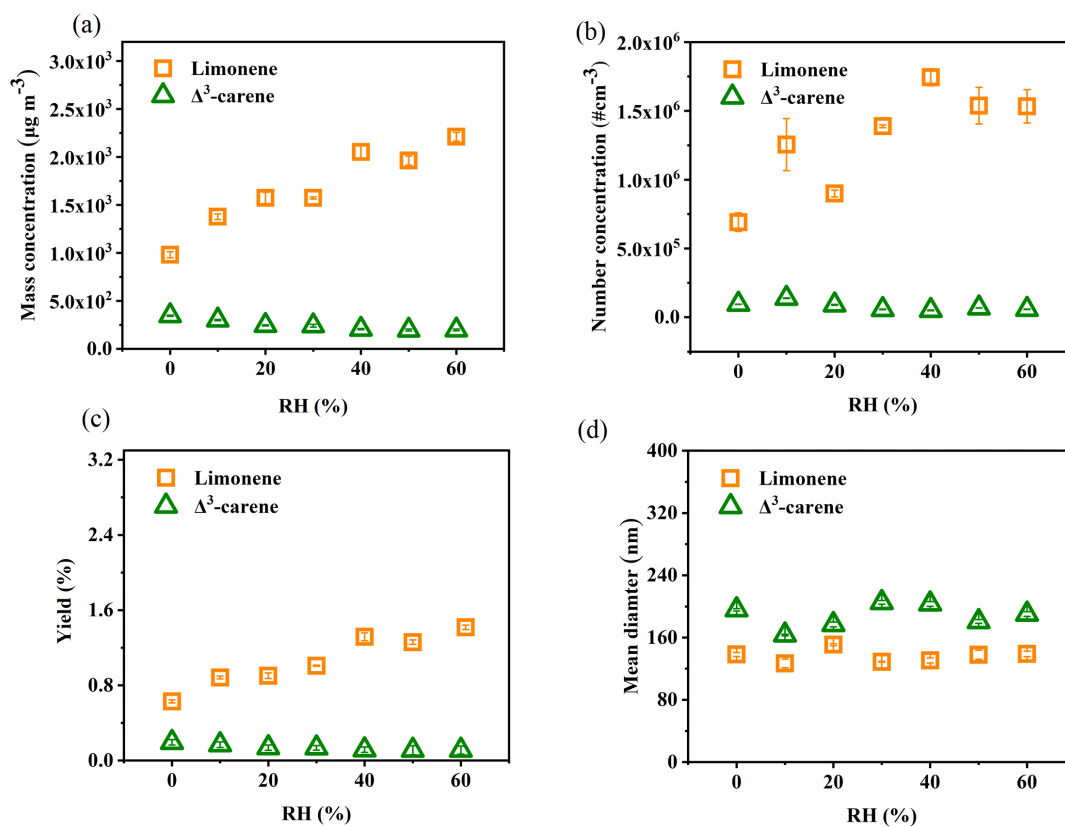
185

186   **Figure 1.** The effect of RH on the SOA formation: (a) number concentration, (b) mass concentration, (c)

187   SOA yield, (d) mean diameter.

188

**Table 2.** Comparison with previous studies on the effect of RH.

Precursor	Precursor concentration (ppb)	O$_3$ concentration (ppb)	Reactor	OH scavenger	T (K)	RH (%)	SOA Mass Concentration (μg/m^3)	SOA Yield (%)	M[a]	N[b]	Reference
limonene	1000	1000	flow reactor	cyclohexane	295±2	0.02 and 32.5	N.M[c]	N.M[c]	no effect	–[e]	Bonn et al. (2002)
	320	100±5	chamber	N.M.[c]	296±2	18±2, 50±3 and 82±2	24; 58; 120	7.0 ± 0.7; 17.4±1.3; 53.4±1.9	+[d] (7 times)	+[d] (8 times)	Yu et al. (2011)
	15 and 30	430.9	flow reactor	2-butanol	298±0.4	< 2-85	2.7-10.5 and 62-229	6.8-26.4 and 77.4-285.7	+[d]	+[d]	Jonsson et al. (2006)
	endocyclic (24.6) and exocyclic (15.2)	endocyclic (270) and exocyclic (12200)	flow reactor	2-butanol	298	10-50	endocyclic (~11) and exocyclic (22-51)	endocyclic (~7.4) and exocyclic (23.8-55.3)	exocyclic (+[d]) and endocyclic (–[c])	N.M[c]	Gong and Chen (2021)
	1085	900±10	flow reactor	none	298	3-62	150; 200; 210	N.M	+[d]	–[e]	Li et al. (2019)

Δ³-carene											
	321±39	5786±203	flow reactor	none	298	0-60	980.9-2211.1	62.9-141.8	+[d] (2 times)	+[d] (3 times)	this study
	1000	1000	flow reactor	cyclohexane	295±2	0.02 and 32.5	N.M[c]	N.M[c]	no effect	–[e]	Bonn et al. (2002)
Δ³-carene	14.2 and 29.4	2300	flow reactor	2-butanol	298±0.4	< 2-85	0.78-3.8 and 15.3-94;	2.1-10.1and 19.8- 116.7	+[d]	+[d]	Jonsson et al. (2006)
	1111	900±10	flow reactor	none	298	3-62	75; 80; 90	N.M	–[e]	–[e]	Li et al. (2019)
	341±28	6257±140	flow reactor	none	298	0-60	346.0-198.5	19.4-11.1	–[e]	no effect	this study

190   [a] M means the change trend total particle mass concentration. [b] N means total particle number concentration. [c] N.M. means not mentioned. [d] Positive sign (+) means the

191   mass or number concentration increases with RH. [e] Negative sign (–) means the mass or number concentration decreases with RH.

3.2 Molecular analysis of SOA particles

The UPLC/ESI-Q-TOF-MS was used to examine the SOA molecular composition under high and low RH conditions. As shown in Fig. 2a, the mass spectra of limonene-SOA are divided into four groups: monomeric group (<m/z 300), dimeric group (m/z 300-500), trimeric group (m/z 500-700), and tetrameric group (m/z 700-1000), corresponding to products containing one, two, three, and four oxygenated limonene units, respectively (Bateman et al., 2009). Most of the SOA molecules are monomers (>60%) (Fig. 2b) and dimers (~25%), while trimers and tetramers contribute to very small fractions (<10% and ~3%) (Table S1). Correspondingly, the distribution of Δ^3-carene-SOA can be divided into four groups (Fig. S4), comparable to that of limonene-SOA. Most of the SOA molecules are monomers (~70%) and dimers (~25%), while trimers and tetramers contribute to smaller proportions (~2% and <1%, respectively) (Table S2). Although the SOA mass concentration increases by ~100% under high RH condition, the relative intensities of MS peaks do not significantly change with varying RH conditions. In other words, we did not observe an obvious change in the overall MS patterns, and the fractions of the four groups only slightly differed under different RH conditions, e.g., the fraction of monomers was 62% under dry condition and 66% under wet conditions. However, if we take a closer look, the intensities and contributions of specific peaks are quite different with varying RH. For example, the relative intensity of $C_{10}H_{16}O_2$, a possible first-generation product (Gong et al., 2018), decreases by ~20% with increasing RH from dry to 60% (Table S3). This is likely due to the multi-generation reactions influenced by water vapor concentration, as discussed below with the proposed reaction mechanism of limonene ozonolysis.
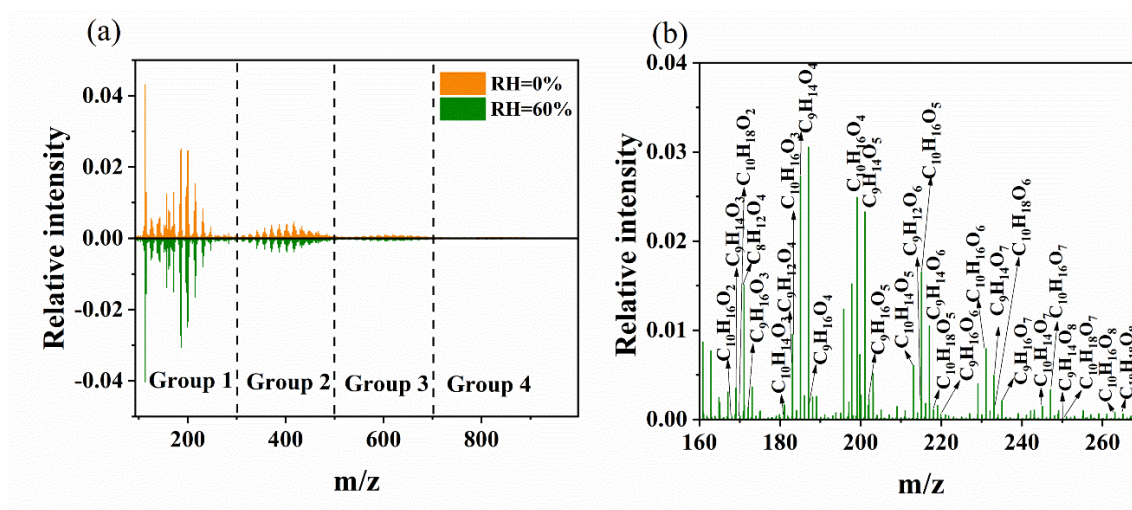
213   **Figure 2.** UPLC/ (−) ESI-Q-TOF-MS mass spectra of SOA from limonene ozonolysis. (a) MS under

214   high and low RH conditions; (b) the identification of monomers under high RH condition.
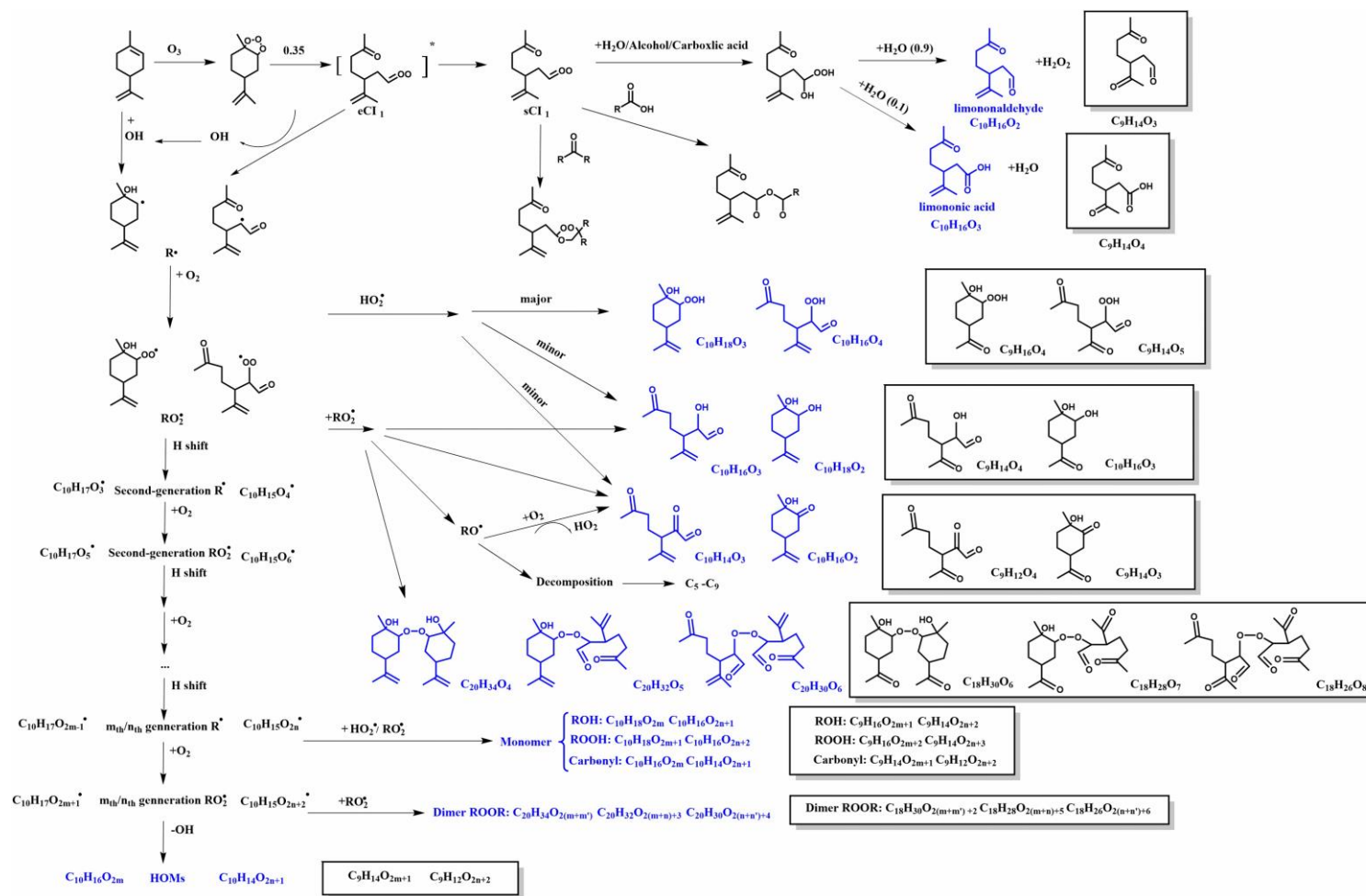
215   The proposed reaction mechanism of limonene ozonolysis is shown in Fig. 3 and Fig. 4. The initial

216   step in the reaction of O_3 with limonene is the attack of the endocyclic double bond to form eCI_1 and

217   eCI_2 (with branching ratios of 0.35 and 0.65, respectively). In the context of eCI_1, several complex

218   reactions occur, with the most dominant reaction being the generation of hydroxyl radicals (OH) and a

219   reaction pathway known as sCI_1. The sCI_1 pathway can proceed through three distinct reactions, as

220   depicted in Fig. 3. The first pathway is the reaction with H_2O, alcohol or carboxylic acid to form a

221   carboxylic acid species with hydroxyl, which would subsequently lose a molecule of water to form

222   limononaldehyde or lose a molecule of hydrogen peroxide to form limononic acid (Grosjean et al., 1992;

223   Li et al., 2019b). The second and third pathways involve reactions of sCI_1 with carboxylic acids and

224   carbonyls, respectively, leading to the formation of anhydrides and secondary ozonides. Additionally, the

225   generated OH radicals can react with limonene, giving rise to another alkyl radical, $C_{10}H_{17}O\cdot$. These

226   alkyl radicals react with O_2 and form peroxy radicals ($RO_2\cdot$). The atmospheric fate of produced $RO_2\cdot$ in

227   the absence of NO_x includes the reaction with $RO_2\cdot$ or $HO_2\cdot$ (Atkinson and Arey, 2003) and the

228   unimolecular H shift. The $RO_2\cdot + HO_2\cdot$ route mainly form hydroperoxide (ROOH), and the minor fraction

229   is to form alcohols and carbonyls (Atkinson and Arey, 2003). The products of bimolecular reactions

230   between $RO_2\cdot$ and $RO_2\cdot$ are alcohols, carbonyls, alkoxy radicals, peroxides and ROOR dimers (Hammes

231   et al., 2019; Peng et al., 2019). The H shift of $RO_2\cdot$ can form second-generation R· and trigger a main

232   generation channel of highly oxidized molecules (HOMs), i.e., R· would go through a process of repeated

233   oxygen addition and hydrogen-atom shift to form HOMs with high O/C ratios of > 0.7–0.8 (Molteni et

234   al., 2018; Bianchi et al., 2019).

235   In addition to the eCI_1 route, the eCI_2 pathway is also responsible for the generation of various

236   products (Fig. 4). Since the reaction of the hydroxyl radical (OH) attacking limonene is already depicted

237   in Fig. 3, our main emphasis in Fig. 4 is on the pathways involved in the generation of SCI. First, sCI_2

238   reacts with H_2O and decomposes to limononaldehyde and H_2O_2. Additionally, sCI_2 could experience an

239   O_2 addition, ·OH loss and isomerization to produce two types of $RO_2\cdot$, which can undergo the similar

240   reactions as the $RO_2\cdot$ formed from the sCI_1 route, and the major products are also shown in Fig. 4.

241   Since limonene and Δ^3-carene both have an endocyclic double bond, the similar reactions as

242   mentioned above can occur for the ozonolysis of Δ^3-carene (Fig. S5), and most corresponding formula

243   in Fig. S5 could be identified in Table S4. However, the reactivity of limonene towards O_3 is expected to

244   be higher owing to its exocyclic double bond. As shown in Fig. 4, the attack of O_3 to the exocyclic double

245   bond mainly leads to sCI_3 (highlighted in red) with the unpaired electrons outside the ring (Leungsakul

246   et al., 2005). sCI_3 can react with H_2O to form a carbonyl called keto-limonene. It should be noted that

247   this reaction can occur not only for limonene, but also for all the products that retain the exocyclic double

248   bond. As a result, the compounds that are colored in blue in Fig. 3 and Fig. 4 can undergo further reactions

249   to generate products with an additional carbonyl (see the boxes in Fig. 3 and Fig. 4). Furthermore, their

250   molecular formula shown in Table S5 have been identified using the Q-TOF-MS. This mechanism can

251   well explain the decrease in the relative intensity of $C_{10}H_{16}O_2$ from high RH to low RH and the increase

252   in the relative intensity of $C_9H_{14}O_3$ from low RH to high RH (Table S3).

253   In such progress, we cannot rule out the possibility that relative humidity (RH) may influence the

254   generation of other free radicals (Ma et al., 2009), thereby impacting the formation of secondary organic

255   aerosols (SOA), such as, OH-radical reactions (Bonn et al., 2002; Fick et al., 2002). However, Molar OH

256   radical yields were reported as 0.65±0.10 (Hantschke et al., 2021), 0.86±0.11 (Aschmann et al., 2002)

257   and 0.56 to 0.59 (Wang et al., 2019) for Δ^3-carene, while for limonene, the reported yields were 0.67±0.10

258   (Aschmann et al., 2002) and 0.76±0.06 (Herrmann et al., 2010). It seems that the OH radicals produced

259   from limonene and Δ^3-carene are quite similar within the range of uncertainties. Therefore, the increased

260   ozone consumption by limonene seems primarily attributed to the presence of its exocyclic double bond.

261

Figure 3. Proposed formation mechanism for SOA formation from eCI$_1$ oxidation under high RH. The compounds in blue and in boxes are identified using UPLC/ (−) ESI-Q-
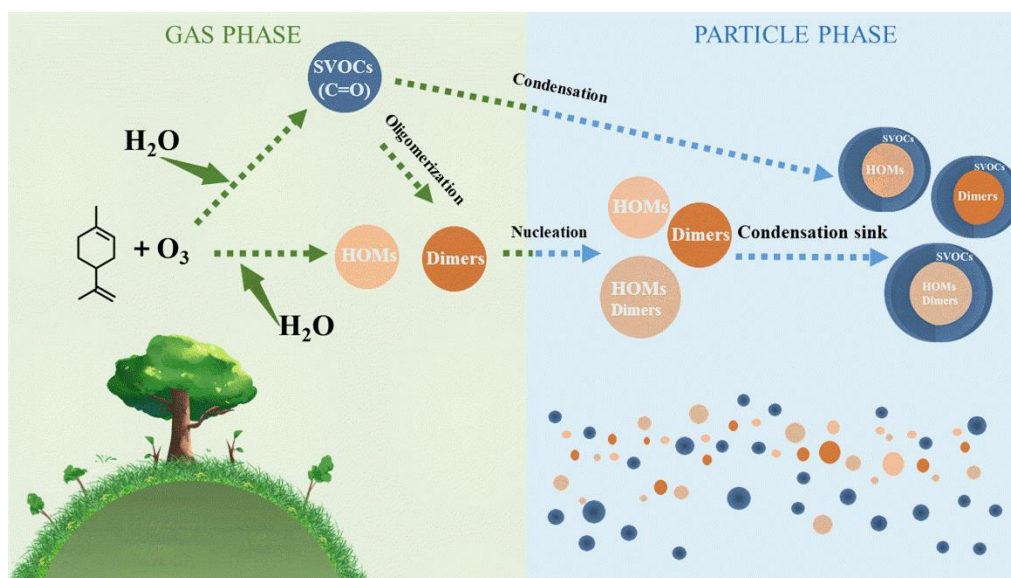
TOF-MS.

264

Figure 4. Proposed formation mechanisms for SOA formation from eCI_2 and exocyclic double bond oxidation under high RH. The compounds in blue and in boxes are identified using UPLC/ (−) ESI-Q-TOF-MS.

3.3 Processes leading to the increase or decrease in SOA formation

Based on the results and mechanisms shown above, we present evidence that high humidity enhances limonene-SOA formation. First, the presence of water vapor enhances the formation of carbonyls from the reaction of exocyclic double bond, and the oligomerization of these carbonyls generates more dimers including hemiacetal (or acetal) formation and aldol condensation (Zhang et al., 2022; Kroll et al., 2005; Jang et al., 2003). As shown in Table S6, the intensity of dimers generating from multi-carbonyls under high RH is higher than that under low RH, and 54 out of the total 187 dimers were exclusively observed for limonene under high humidity conditions, contributing to a corresponding intensity of ~19% (Table S7). These dimers can be classified as low-volatile organic compounds (LVOC; $3 \times 10^{-4} < C_0 < 0.3$ μg m^{-3}) and extremely low-volatile organic compounds (ELVOCs; $C_0 < 3 \times 10^{-4}$ μg m^{-3}) (Fig. 5a), and thus promote the nucleation and new particle formation in different ways. This finding is similar to that from a previous study showing that high RH can promote dimer formation from the ozonolysis of α-pinene (Kristensen et al., 2014). Second, we find that high RH can also promote the formation of HOMs, although the mechanism remains unclear. As shown in Table S3, many HOMs proposed from the mechanism are detected under high RH condition but not detected under low RH condition, including both monomers and dimers. Many HOMs have low volatilities and, thus, can also promote new particle formation. Overall, the promoted dimer and HOM formation may greatly enhance the new particle number concentration under high RH condition (Fig. 6).

15

287

288 **Figure 5.** (a) Distribution of the limonene-SOA in the two-dimensional volatility basis set (2D-VBS)

289 space. (b) Partitioning coefficients of limonene monomers and dimers under low and high RH conditions.

290

291

292 **Figure 6.** Schematic diagram of the possible mechanisms for the enhancement of limonene-SOA.

293

294   High particle number concentration generally provides more surface areas for semi-volatile organic

295 compounds (SVOCs; $0.3 < C_0 < 300$ µg m^{-3}) to condense on, which results in higher condensation sink

296 (CS). In the OFR, the fates of SVOCs include condensing on aerosol, getting lost on the wall, and reacting

297 with OH radicals to form functionalization and/or fragmentation products (Palm et al., 2016; Li et al.,

298 2019a). The promoted condensation by higher CS leads to a higher fraction of SVOCs getting into the

299 particle phase rather than getting lost on the wall or becoming smaller fragments staying in the gas phase,

16

300 and thus promoting SOA formation (Li et al., 2019a). Furthermore, the transformation from C-C double

301 bond to carbonyl shown in Fig. 3 and Fig. 4 decreases the volatility of molecules, which can largely

302 influence the gas-particle partitioning of the monomeric compounds (Fig. 5b). For example, the C_0 values

303 of $C_{10}H_{16}O_2$ and $C_{10}H_{16}O_3$ are 90701 and 19968 µg m^{-3}, corresponding to partitioning coefficients of

304 0.01 and 0.05, respectively (Fig. 5b and Table S3), with an SOA mass concentration of ~1000 µg m^{-3}

305 under dry condition. When they are converted to carbonyls $C_9H_{14}O_3$ and $C_9H_{14}O_4$, the values of C_0

306 become 45556 and 6479 µg m^{-3}, corresponding to partitioning coefficients of 0.02 and 0.13, respectively

307 (Fig. 5b and Table S3), with the same SOA loading. This enhancement in partitioning coefficient can

308 largely promote the condensation of SVOCs and, thus, enhance the SOA mass concentration. In addition,

309 the enhanced SOA formation can further influence the equilibrium, e.g., the partitioning coefficient of

310 $C_{10}H_{16}O_3$ increases from 0.05 to 0.10 when SOA mass concentration increases from ~1000 µg m^{-3} under

311 dry condition to ~2000 µg m^{-3} under wet condition (Fig. 5b and Table S3). The distribution of saturation

312 vapor pressure for monomers and dimers identified by MS has also been shown in Fig. 5a. As can be

313 seen from this figure, around 50% monomers are categorized as SVOCs, thus having the large fraction

314 in the particle phase when converting from dry to wet conditions. Overall, it is likely that the different

315 fate and partitioning of SVOCs largely enhance the amount of SVOCs in the particle phase (Fig. 6).

316 Concluding the analysis above, high humidity promotes the SOA formation from the ozonolysis of

317 limonene in two steps: nucleation of new particles and condensation of SVOCs on them (Fig. 6). While

318 our study highlights significant changes in gas-phase chemistry, we cannot exclude the possibility of

319 concurrent reactions occurring in the condensed phase. These two steps are closely related to the multi-

320 generation reactions of the exocyclic C=C bond, which are unlikely to happen for the ozonolysis of Δ^3-

321 carene. Interestingly, Gong and Chen (2021) have found that high RH can inhibit the SOA formation

322 from the first-generation oxidation of limonene ozonolysis, but enhance the SOA formation from the

323 second-generation oxidation (Gong and Chen, 2021), their results agree well with the results and analysis

324 shown here. In contrast, Li et al. (2019b) found negligible change in dimers and HOMs in limonene-O_3

325 system when changing RH from 0 to 60%. The discrepancy is mainly attributed to the different

326 experimental conditions. The ozone exposure in this study is ~18 times higher than in Li et al. (2019b),

327 while the limonene concentration in this study is only ~30% of that in their study. These two conditions

328 both favor the multi-generation reactions occurred at the exocyclic double bond of limonene and its

329   products. Thus, we believe this leads to the different results regarding the formation of HOMs and dimers.

330   Regarding Δ^3-carene, the mechanisms and processes are almost opposite to those of limonene. First,

331   water vapor reacts with sCI_1 or sCI_2 to promote the formation of α-hydroxyalkyl-hydroperoxides (Fig.

332   S5). Their subsequent products without second ozonolysis of exocyclic double bond have higher

333   volatility, and may most likely prevail in the gas phase. In addition, it has been found that α-hydroxyalkyl

334   hydroperoxides preferentially decompose into aldehydes and H_2O_2 (Kumar et al., 2014; Chen et al., 2016),

335   i.e., 3-caronaldehyde for Δ^3-carene, which has higher volatility than the products from other reaction

336   pathways. Correspondingly, the number and relative intensity of HOMs and dimers detected under high

337   RH conditions are both lower than those under low RH conditions (Table S8). Furthermore, out of a total

338   of 178 dimers, 63 dimers were exclusively identified under low RH conditions (Table S7). As a result,

339   high RH shows an inhibitory effect on the SOA formation from Δ^3-carene ozonolysis.

340   To investigate the multi-generation reactions of limonene under low-concentration conditions, we

341   conducted low-concentration limonene ozonolysis experiments, and the results are shown in Fig. S6. In

342   these experiments, the limonene and O_3 concentrations were 20.5 ppb and 5.7 ppm, respectively.

343   According to the experimental results, the number concentration of SOA formed from limonene

344   ozonolysis increased by approximately 1.4 times under high RH, which is similar to the increase observed

345   under high-loading conditions. The mass concentration increased by approximately 1.3 times at a

346   precursor concentration of 20.5 ppb. The relatively small increase in mass concentration compared to the

347   high-concentration conditions may be attributed to the less pronounced distribution of SVOCs at low

348   mass concentrations. This result suggests that the enhancement effect on limonene SOA by high RH is

349   still valid for low precursor concentrations.

350   To further confirm the assumption that water-influenced multi-generation reactions of the exocyclic

351   double bond enhance the SOA formation, we conducted two comparative analyses: firstly, we examined

352   the ozonolysis of the endocyclic double bond in limonene, leaving the exocyclic double bond unreacted.

353   This was done by applying a low O_3 concentration (~67 ppb), since the reaction of O_3 with endocyclic

354   double bond is ~30 times faster than the reaction of O_3 with exocyclic double bond (Shu and Atkinson,

355   1994). Interestingly, when limonene was oxidized at only the endocyclic double bond, we observed a

356   slight decrease in both the number and mass concentrations as the RH increased (Fig. S7). This is similar

357   to the results obtained for Δ^3-carene, which contains only one endocyclic double bond. Secondly, we

358   compared the ozonolysis of structurally similar β-caryophyllene, which has an exocyclic C-C double

359   bond that can undergo further reactions (Fig. S8). As expected, we observe a large enhancement in SOA

360   formation under high RH condition (Table S9 and Fig. S9). This implies that monoterpenes,

361   sesquiterpenes, and other BVOCs with two unsaturation double bonds may follow similar reaction

362   mechanisms during ozonolysis, and thus have a RH dependency in SOA production.

363   **4 Conclusions**

364   In this study, the effect of humidity on SOA production from the ozonolysis of two monoterpenes

365   (limonene and Δ^3-carene) was investigated with an OFR. Contrasting impacts of RH on the SOA

366   formation were observed: limonene-SOA yield increases by ~100% when RH changes from ~1% to

367   ~60%, while Δ^3-carene-SOA yield slightly decreases. By analyzing the chemical composition of SOA

368   with ESI-Q-TOF-MS, we find that the multi-generation reactions of the exocyclic C-C double bond are

369   likely the driving force of the enhancement in limonene-SOA. The presence of water promotes the

370   formation of carbonyls from the reaction of exocyclic double bond, and further favors the formation of

371   dimers and HOMs. This leads to promoted new particle formation and subsequent condensation of

372   SVOCs. These reactions also lower the volatilities of the SVOCs, and further promote the gas-particle

373   partitioning. Moreover, this hypothesis is supported by a similar behavior of the ozonolysis of β-

374   caryophyllene (sesquiterpene with an exocyclic double bond) in SOA enhancement under high RH

375   condition. However, since aerosol dynamics of small clusters and particles are very complex, we do not

376   rule out a series of reactions that may occur in the particle phase. The results in this study suggest that

377   multi-generation reactions play an important role in SOA formation from the ozonolysis of BVOCs,

378   which are significantly influenced by humidity. This impact is largely dependent on the molecular

379   structure of the SOA precursors (e.g., with or without the exocyclic double bond), thus highlighting the

380   importance to consider the molecular structure of monoterpenes in modeling and field studies of biogenic

381   SOA.

382

383   **Data availability.** Experimental data are available upon request to the corresponding authors.

384   **Supplement.** The supplement related to this article is available online.

385   **Author contributions.** LD and SZ designed the experiments and SZ carried them out. SZ performed

394   **Reference**

395   Ahmadov, R., McKeen, S. A., Robinson, A. L., Bahreini, R., Middlebrook, A. M., de Gouw, J. A.,

396   Meagher, J., Hsie, E. Y., Edgerton, E., Shaw, S., and Trainer, M.: A volatility basis set model for

397   summertime secondary organic aerosols over the eastern United States in 2006, J. Geophys. Res.-Atmos.,

398   117, D6301, https://doi.org/10.1029/2011JD016831, 2012.

399   Aschmann, S. M., Arey, J., and Atkinson, R.: OH radical formation from the gas-phase reactions of O3

400   with a series of terpenes, Atmos. Environ., 36, 4347-4355, https://doi.org/10.1016/S1352-

401   2310(02)00355-2, 2002.

402   Atkinson, R.: Kinetics and mechanisms of the gas-phase reactions of the NO_3 radical with organic

403   compounds, J. Phys. Chem. Ref. Data, 20, 459-507, https://doi.org/10.1063/1.555887, 1991.

404   Atkinson, R. and Arey, J.: Gas-phase tropospheric chemistry of biogenic volatile organic compounds: a

405   review, Atmos. Environ., 37, 197-219, https://doi.org/10.1016/S1352-2310(03)00391-1, 2003.

406   Bäck, J., Aalto, J., Henriksson, M., Hakola, H., He, Q., and Boy, M.: Chemodiversity of a Scots pine

407   stand   and   implications   for   terpene   air   concentrations,   Biogeosciences,   9,   689-702,

408   https://doi.org/10.5194/bg-9-689-2012, 2012.

409   Bateman, A. P., Nizkorodov, S. A., Laskin, J., and Laskin, A.: Time-resolved molecular characterization

410   of limonene/ozone aerosol using high-resolution electrospray ionization mass spectrometry, Phys. Chem.

411   Chem. Phys., 11, 7931-7942, https://doi.org/10.1039/b905288g, 2009.

412   Bianchi, F., Kurtén, T., Riva, M., Mohr, C., Rissanen, M. P., Roldin, P., Berndt, T., Crounse, J. D.,

413   Wennberg, P. O., Mentel, T. F., Wildt, J., Junninen, H., Jokinen, T., Kulmala, M., Worsnop, D. R.,

Thornton, J. A., Donahue, N., Kjaergaard, H. G., and Ehn, M.: Highly oxygenated organic molecules (HOM) from gas-phase autoxidation involving peroxy radicals: a key contributor to atmospheric aerosol, Chem. Rev., 119, 3472-3509, https://doi.org/10.1021/acs.chemrev.8b00395, 2019.

Bonn, B. and Moortgat, G. K.: New particle formation during α- and β-pinene oxidation by O_3, OH and NO_3, and the influence of water vapour: particle size distribution studies, Atmos. Chem. Phys., 2, 183-196, https://doi.org/10.5194/acp-2-183-2002, 2002.

Bonn, B., Schuster, G., and Moortgat, G. K.: Influence of water vapor on the process of new particle formation during monoterpene ozonolysis, J. Phys. Chem. A, 106, 2869-2881, https://doi.org/10.1021/jp012713p, 2002.

Chen, H., Ren, Y., Cazaunau, M., Dalele, V., Hu, Y., Chen, J., and Mellouki, A.: Rate coefficients for the reaction of ozone with 2-and 3-carene, Chem. Phys. Lett., 621, 71-77, https://doi.org/10.1016/j.cplett.2014.12.056, 2015.

Chen, L., Huang, Y., Xue, Y., Shen, Z., Cao, J., and Wang, W.: Mechanistic and kinetics investigations of oligomer formation from Criegee intermediate reactions with hydroxyalkyl hydroperoxides, Atmos. Chem. Phys., 19, 4075-4091, https://doi.org/10.5194/acp-19-4075-2019, 2019.

Chen, L., Wang, W., Wang, W., Liu, Y., Liu, F., Liu, N., and Wang, B.: Water-catalyzed decomposition of the simplest Criegee intermediate CH_2OO, Theor. Chem. Acc., 135, 131, https://doi.org/10.1007/s00214-016-1894-9, 2016.

Chen, X. and Hopke, P. K.: A chamber study of secondary organic aerosol formation by limonene ozonolysis, Indoor Air, 20, 320-328, https://doi.org/10.1111/j.1600-0668.2010.00656.x, 2010.

Cholakian, A., Beekmann, M., Coll, I., Ciarelli, G., and Colette, A.: Biogenic secondary organic aerosol sensitivity to organic aerosol simulation schemes in climate projections, Atmos. Chem. Phys., 19, 13209-13226, https://doi.org/10.5194/acp-19-13209-2019, 2019.

de Matos, S. P., Teixeira, H. F., de Lima, Á. A. N., Veiga-Junior, V. F., and Koester, L. S.: Essential oils and isolated terpenes in nanosystems designed for topical administration: a review, Biomolecules, 9, 138, https://doi.org/doi:10.3390/biom9040138, 2019.

Drozd, G. T. and Donahue, N. M.: Pressure dependence of stabilized Criegee intermediate formation from a sequence of alkenes, J. Phys. Chem. A, 115, 4381-4387, https://doi.org/10.1021/jp2001089, 2011.

Fick, J., Pommer, L., Andersson, B., and Nilsson, C.: A study of the gas-phase ozonolysis of terpenes:

443   the impact of radicals formed during the reaction, Atmos. Environ., 36, 3299-3308,

444   https://doi.org/10.1016/s1352-2310(02)00291-1, 2002.

445   Gong, Y. and Chen, Z.: Quantification of the role of stabilized Criegee intermediates in the formation of

446   aerosols in limonene ozonolysis, Atmos. Chem. Phys., 21, 813-829, https://doi.org/10.5194/acp-21-813-

447   2021, 2021.

448   Gong, Y., Chen, Z., and Li, H.: The oxidation regime and SOA composition in limonene ozonolysis: roles

449   of different double bonds, radicals, and water, Atmos. Chem. Phys., 18, 15105-15123,

450   https://doi.org/10.5194/acp-18-15105-2018, 2018.

451   Grosjean, D., Williams, E. L., and Seinfeld, J. H.: Atmospheric oxidation of selected terpenes and related

452   carbonyls: gas-phase carbonyl products, Environ. Sci. Technol., 26, 1526-1533,

453   https://doi.org/10.1021/es00032a005, 1992.

454   Guenther, A. B., Jiang, X., Heald, C. L., Sakulyanontvittaya, T., Duhl, T., Emmons, L. K., and Wang, X.:

455   The model of emissions of gases and aerosols from nature version 2.1 (MEGAN2.1): an extended and

456   updated framework for modeling biogenic emissions, Geosci. Model Dev., 5, 1471-1492,

457   https://doi.org/10.5194/gmd-5-1471-2012, 2012.

458   Guo, S., Hu, M., Zamora, M. L., Peng, J., Shang, D., Zheng, J., Du, Z., Wu, Z., Shao, M., Zeng, L.,

459   Molina, M. J., and Zhang, R.: Elucidating severe urban haze formation in China, Proc. Natl. Acad. Sci.

460   U. S. A., 111, 17373-17378, https://doi.org/10.1073/pnas.1419604111, 2014.

461   Hammes, J., Lutz, A., Mentel, T., Faxon, C., and Hallquist, M.: Carboxylic acids from limonene oxidation

462   by ozone and hydroxyl radicals: insights into mechanisms derived using a FIGAERO-CIMS, Atmos.

463   Chem. Phys., 19, 13037-13052, https://doi.org/10.5194/acp-19-13037-2019, 2019.

464   Hantschke, L., Novelli, A., Bohn, B., Cho, C., Reimer, D., Rohrer, F., Tillmann, R., Glowania, M.,

465   Hofzumahaus, A., Kiendler-Scharr, A., Wahner, A., and Fuchs, H.: Atmospheric photooxidation and

466   ozonolysis of Δ3-carene and 3-caronaldehyde: rate constants and product yields, Atmos. Chem. Phys.,

467   21, 12665-12685, 10.5194/acp-21-12665-2021, 2021.

468   Herrmann, F., Winterhalter, R., Moortgat, G. K., and Williams, J.: Hydroxyl radical (OH) yields from the

469   ozonolysis of both double bonds for five monoterpenes, Atmos. Environ., 44, 3458-3464,

470   https://doi.org/10.1016/j.atmosenv.2010.05.011, 2010.

471   Huang, X., Yun, H., Gong, Z., Li, X., He, L., Zhang, Y., and Hu, M.: Source apportionment and secondary

organic aerosol estimation of PM2.5 in an urban atmosphere in China, Sci. China-Earth Sci., 57, 1352-1362, https://doi.org/10.1007/s11430-013-4686-2, 2014.

Jang, M. S., Carroll, B., Chandramouli, B., and Kamens, R. M.: Particle growth by acid-catalyzed heterogeneous reactions of organic carbonyls on preexisting aerosols, Environ. Sci. Technol., 37, 3828-3837, 10.1021/es021005u, 2003.

Jokinen, T., Berndt, T., Makkonen, R., Kerminen, V.-M., Junninen, H., Paasonen, P., Stratmann, F., Herrmann, H., Guenther, A. B., Worsnop, D. R., Kulmala, M., Ehn, M., and Sipilä, M.: Production of extremely low volatile organic compounds from biogenic emissions: Measured yields and atmospheric implications, Proc. Natl. Acad. Sci. U. S. A., 112, 7123-7128, https://doi.org/doi:10.1073/pnas.1423977112, 2015.

Jonsson, A. M., Hallquist, M., and Ljungstrom, E.: Impact of humidity on the ozone initiated oxidation of limonene, Δ^3-carene, and α-pinene, Environ. Sci. Technol., 40, 188-194, https://doi.org/10.1021/es051163w, 2006a.

Jonsson, A. M., Hallquist, M., and Ljungstrom, E.: Impact of humidity on the ozone initiated oxidation of limonene, Delta(3)-carene, and alpha-pinene, Environ. Sci. Technol., 40, 188-194, https://doi.org/10.1021/es051163w, 2006b.

Jonsson, A. M., Hallquist, M., and Ljungstrom, E.: Influence of OH scavenger on the water effect on secondary organic aerosol formation from ozonolysis of limonene, Δ^3-carene, and α-pinene, Environ. Sci. Technol., 42, 5938-5944, https://doi.org/10.1021/es702508y, 2008.

Kanakidou, M., Seinfeld, J. H., Pandis, S. N., Barnes, I., Dentener, F. J., Facchini, M. C., Van Dingenen, R., Ervens, B., Nenes, A., Nielsen, C. J., Swietlicki, E., Putaud, J. P., Balkanski, Y., Fuzzi, S., Horth, J., Moortgat, G. K., Winterhalter, R., Myhre, C. E. L., Tsigaridis, K., Vignati, E., Stephanou, E. G., and Wilson, J.: Organic aerosol and global climate modelling: a review, Atmos. Chem. Phys., 5, 1053-1123, https://doi.org/10.5194/acp-5-1053-2005, 2005.

Khamaganov, V. G. and Hites, R. A.: Rate constants for the gas-phase reactions of ozone with isoprene, α- and β-pinene, and limonene as a function of temperature, J. Phys. Chem. A, 105, 815-822, https://doi.org/10.1021/jp002730z, 2001.

Kristensen, K., Cui, T., Zhang, H., Gold, A., Glasius, M., and Surratt, J. D.: Dimers in α-pinene secondary organic aerosol: effect of hydroxyl radical, ozone, relative humidity and aerosol acidity, Atmos. Chem.

Phys., 14, 4201-4218, https://doi.org/10.5194/acp-14-4201-2014, 2014.

Kroll, J. H., Ng, N. L., Murphy, S. M., Varutbangkul, V., Flagan, R. C., and Seinfeld, J. H.: Chamber studies of secondary organic aerosol growth by reactive uptake of simple carbonyl compounds, J. Geophys. Res.-Atmos., 110, 10.1029/2005JD006004, 2005.

Kumar, M., Busch, D. H., Subramaniam, B., and Thompson, W. H.: Role of tunable acid catalysis in decomposition of α-Hydroxyalkyl hydroperoxides and mechanistic implications for tropospheric chemistry, J. Phys. Chem. A, 118, 9701-9711, https://doi.org/10.1021/jp505100x, 2014.

Leungsakul, S., Jaoui, M., and Kamens, R. M.: Kinetic Mechanism for Predicting Secondary Organic Aerosol Formation from the Reaction of d-Limonene with Ozone, Environ. Sci. Technol., 39, 9583-9594, https://doi.org/10.1021/es0492687, 2005.

Levy, H., II, Horowitz, L. W., Schwarzkopf, M. D., Ming, Y., Golaz, J.-C., Naik, V., and Ramaswamy, V.: The roles of aerosol direct and indirect effects in past and future climate change, J. Geophys. Res.-Atmos., 118, 4521-4532, https://doi.org/10.1002/jgrd.50192, 2013.

Li, J. Y., Zhang, H. W., Ying, Q., Wu, Z. J., Zhang, Y. L., Wang, X. M., Li, X. H., Sun, Y. L., Hu, M., Zhang, Y. H., and Hu, J. L.: Impacts of water partitioning and polarity of organic compounds on secondary organic aerosol over eastern China, Atmos. Chem. Phys., 20, 7291-7306, https://doi.org/10.5194/acp-20-7291-2020, 2020.

Li, K., Liggio, J., Lee, P., Han, C., Liu, Q., and Li, S.-M.: Secondary organic aerosol formation from α-pinene, alkanes, and oil-sands-related precursors in a new oxidation flow reactor, Atmos. Chem. Phys., 19, 9715-9731, https://doi.org/10.5194/acp-19-9715-2019, 2019a.

Li, X., Chee, S., Hao, J., Abbatt, J. P. D., Jiang, J., and Smith, J. N.: Relative humidity effect on the formation of highly oxidized molecules and new particles during monoterpene oxidation, Atmos. Chem. Phys., 19, 1555-1570, https://doi.org/10.5194/acp-19-1555-2019, 2019b.

Liu, Q., Liggio, J., Breznan, D., Thomson, E. M., Kumarathasan, P., Vincent, R., Li, K., and Li, S.-M.: Oxidative and Toxicological Evolution of Engineered Nanoparticles with Atmospherically Relevant Coatings, Environ. Sci. Technol., 53, 3058-3066, 10.1021/acs.est.8b06879, 2019.

Liu, Y., Liggio, J., Harner, T., Jantunen, L., Shoeib, M., and Li, S.-M.: Heterogeneous OH Initiated Oxidation: A Possible Explanation for the Persistence of Organophosphate Flame Retardants in Air, Environ. Sci. Technol., 48, 1041-1048, 10.1021/es404515k, 2014.

Ma, Y., Porter, R. A., Chappell, D., Russell, A. T., and Marston, G.: Mechanisms for the formation of organic acids in the gas-phase ozonolysis of 3-carene, Phys. Chem. Chem. Phys., 11, 4184-4197, https://doi.org/10.1039/b818750a, 2009.

Molteni, U., Bianchi, F., Klein, F., El Haddad, I., Frege, C., Rossi, M. J., Dommen, J., and Baltensperger, U.: Formation of highly oxygenated organic molecules from aromatic compounds, Atmos. Chem. Phys., 18, 1909-1921, https://doi.org/10.5194/acp-18-1909-2018, 2018.

Mot, M.-D., Gavrilaș, S., Lupitu, A. I., Moisa, C., Chambre, D., Tit, D. M., Bogdan, M. A., Bodescu, A.-M., Copolovici, L., Copolovici, D. M., and Bungau, S. G.: Salvia officinalis L. essential oil: characterization, antioxidant properties, and the effects of aromatherapy in adult patients, Antioxidants, 11, 808, https://doi.org/10.3390/antiox11050808, 2022.

Ng, N. L., Kroll, J. H., Chan, A. W. H., Chhabra, P. S., Flagan, R. C., and Seinfeld, J. H.: Secondary organic aerosol formation from m-xylene, toluene, and benzene, Atmos. Chem. Phys., 7, 3909-3922, https://doi.org/10.5194/acp-7-3909-2007, 2007.

Odum, J. R., Hoffmann, T., Bowman, F., Collins, D., Flagan, R. C., and Seinfeld, J. H.: Gas/particle partitioning and secondary organic aerosol yields, Environ. Sci. Technol., 30, 2580-2585, https://doi.org/10.1021/es950943+, 1996.

Palm, B. B., Campuzano-Jost, P., Ortega, A. M., Day, D. A., Kaser, L., Jud, W., Karl, T., Hansel, A., Hunter, J. F., Cross, E. S., Kroll, J. H., Peng, Z., Brune, W. H., and Jimenez, J. L.: In situ secondary organic aerosol formation from ambient pine forest air using an oxidation flow reactor, Atmos. Chem. Phys., 16, 2943-2970, https://doi.org/10.5194/acp-16-2943-2016, 2016.

Pathak, R. K., Salo, K., Emanuelsson, E. U., Cai, C., Lutz, A., Hallquist, A. M., and Hallquist, M.: Influence of ozone and radical chemistry on limonene organic aerosol production and thermal characteristics, Environ. Sci. Technol., 46, 11660-11669, https://doi.org/10.1021/es301750r, 2012.

Peng, Z., Lee-Taylor, J., Orlando, J. J., Tyndall, G. S., and Jimenez, J. L.: Organic peroxy radical chemistry in oxidation flow reactors and environmental chambers and their atmospheric relevance, Atmos. Chem. Phys., 19, 813-834, https://doi.org/10.5194/acp-19-813-2019, 2019.

Pye, H. O. T., Ward-Caviness, C. K., Murphy, B. N., Appel, K. W., and Seltzer, K. M.: Secondary organic aerosol association with cardiorespiratory disease mortality in the United States, Nat. Commun., 12, https://doi.org/10.1038/s41467-021-27484-1, 2021.

Ravichandran, C., Badgujar, P. C., Gundev, P., and Upadhyay, A.: Review of toxicological assessment of d-limonene, a food and cosmetics additive, Food Chem. Toxicol., 120, 668-680, https://doi.org/10.1016/j.fct.2018.07.052, 2018.

Sbai, S. E. and Farida, B.: Photochemical aging and secondary organic aerosols generated from limonene in an oxidation flow reactor, Environ. Sci. Pollut. Res., 26, 18411-18420, https://doi.org/10.1007/s11356-019-05012-5, 2019.

Seinfeld, J. H., Erdakos, G. B., Asher, W. E., and Pankow, J. F.: Modeling the formation of secondary organic aerosol (SOA). 2. The predicted effects of relative humidity on aerosol formation in the α-Pinene-, β-Pinene-, sabinene-, Δ^3-Carene-, and cyclohexene-ozone systems, Environ. Sci. Technol., 35, 1806-1817, https://doi.org/10.1021/es001765+, 2001.

Shaw, J. T., Lidster, R. T., Cryer, D. R., Ramirez, N., Whiting, F. C., Boustead, G. A., Whalley, L. K., Ingham, T., Rickard, A. R., Dunmore, R. E., Heard, D. E., Lewis, A. C., Carpenter, L. J., Hamilton, J. F., and Dillon, T. J.: A self-consistent, multivariate method for the determination of gas-phase rate coefficients, applied to reactions of atmospheric VOCs and the hydroxyl radical, Atmos. Chem. Phys., 18, 4039-4054, https://doi.org/10.5194/acp-18-4039-2018, 2018.

Shu, Y. G. and Atkinson, R.: Rate Constants for the gas-pahse reactions of O_3 with a series of terpenes and OH radical formation from the O_3 reactions with sesquiterpenes at 296 ±2K, Int. J. Chem. Kinet., 26, 1193-1205, 10.1002/kin.550261207, 1994.

Sindelarova, K., Granier, C., Bouarar, I., Guenther, A., Tilmes, S., Stavrakou, T., Müller, J. F., Kuhn, U., Stefani, P., and Knorr, W.: Global data set of biogenic VOC emissions calculated by the MEGAN model over the last 30 years, Atmos. Chem. Phys., 14, 9317-9341, https://doi.org/10.5194/acp-14-9317-2014, 2014.

Sun, Y., Wang, Z., Fu, P., Jiang, Q., Yang, T., Li, J., and Ge, X.: The impact of relative humidity on aerosol composition and evolution processes during wintertime in Beijing, China, Atmos. Environ., 77, 927-934, https://doi.org/10.1016/j.atmosenv.2013.06.019, 2013.

Thomsen, D., Elm, J., Rosati, B., Skonager, J. T., Bilde, M., and Glasius, M.: Large discrepancy in the formation of secondary organic aerosols from structurally similar monoterpenes, ACS Earth Space Chem., 5, 632-644, https://doi.org/10.1021/acsearthspacechem.0c00332, 2021.

Varutbangkul, V., Brechtel, F. J., Bahreini, R., Ng, N. L., Keywood, M. D., Kroll, J. H., Flagan, R. C.,

588 Seinfeld, J. H., Lee, A., and Goldstein, A. H.: Hygroscopicity of secondary organic aerosols formed by

589 oxidation of cycloalkenes, monoterpenes, sesquiterpenes, and related compounds, Atmos. Chem. Phys.,

590 6, 2367-2388, https://doi.org/10.5194/acp-6-2367-2006, 2006.

591 Wang, L., Liu, Y., and Wang, L.: Ozonolysis of 3-carene in the atmosphere. Formation mechanism of

592 hydroxyl radical and secondary ozonides, Phys. Chem. Chem. Phys., 21, 8081-8091,

593 10.1039/c8cp07195k, 2019.

594 Wang, L. Y. and Wang, L. M.: The oxidation mechanism of gas-phase ozonolysis of limonene in the

595 atmosphere, Phys. Chem. Chem. Phys., 23, 9294-9303, https://doi.org/10.1039/d0cp05803c, 2021.

596 Watne, A. K., Westerlund, J., Hallquist, A. M., Brune, W. H., and Hallquist, M.: Ozone and OH-induced

597 oxidation of monoterpenes: Changes in the thermal properties of secondary organic aerosol (SOA), J.

598 Aerosol Sci, 114, 31-41, https://doi.org/10.1016/j.jaerosci.2017.08.011, 2017.

599 Xu, L., Tsona, N. T., and Du, L.: Relative humidity changes the role of SO_2 in biogenic secondary organic

600 aerosol formation, J. Phys. Chem. Lett., 12, 7365-7372, https://doi.org/10.1021/acs.jpclett.1c01550,

601 2021.

602 Ye, J., Abbatt, J. P. D., and Chan, A. W. H.: Novel pathway of SO_2 oxidation in the atmosphere: reactions

603 with monoterpene ozonolysis intermediates and secondary organic aerosol, Atmos. Chem. Phys., 18,

604 5549-5565, https://doi.org/10.5194/acp-18-5549-2018, 2018.

605 Yu, K. P., Lin, C. C., Yang, S. C., and Zhao, P.: Enhancement effect of relative humidity on the formation

606 and regional respiratory deposition of secondary organic aerosol, J. Hazard. Mater., 191, 94-102,

607 https://doi.org/10.1016/j.jhazmat.2011.04.042, 2011.

608 Zhang, H., Wang, S., Hao, J., Wang, X., Wang, S., Chai, F., and Li, M.: Air pollution and control action

609 in Beijing, J. Clean Prod., 112, 1519-1527, https://doi.org/10.1016/j.jclepro.2015.04.092, 2016.

610 Zhang, Y., He, L., Sun, X., Ventura, O. N., and Herrmann, H.: Theoretical Investigation on the

611 Oligomerization of Methylglyoxal and Glyoxal in Aqueous Atmospheric Aerosol Particles, ACS Earth

612 Space Chem., 6, 1031-1043, 10.1021/acsearthspacechem.1c00422, 2022.

613 Zhao, R. R., Zhang, Q. X., Xu, X. Z., Zhao, W. X., Yu, H., Wang, W. J., Zhang, Y. M., and Zhang, W. J.:

614 Effect of experimental conditions on secondary organic aerosol formation in an oxidation flow reactor,

615 Atmos. Pollut. Res., 12, 392-400, https://doi.org/10.1016/j.apr.2021.01.011, 2021.

616 Ziemann, P. J. and Atkinson, R.: Kinetics, products, and mechanisms of secondary organic aerosol

617   formation, Chem. Soc. Rev., 41, 6582-6605, https://doi.org/10.1039/c2cs35122f, 2012.

618

Supplement of

Contrasting impacts of humidity on the ozonolysis of monoterpenes: insights into the multi-generation chemical mechanism

Shan Zhang et al.

Correspondence to: Lin Du (lindu@sdu.edu.cn) and Kun Li (kun.li@sdu.edu.cn)

Section S1. Calculation of equivalent aging days

The equivalent aging days can be calculated by $\text{Age (days)}=k\frac{O_{3\text{exp}}}{[O_3]}=k\frac{[O_3]_0\times RT}{[O_3]}$, where $[O_3]_0$ is the initial ozone concentration in OFR, RT is the residence time, k is a constant coefficient which is equals to 1.03 and $[O_3]$ is the mean ozone concentration in the atmosphere for 1 day, estimated to be 6.05×10^{16} molec cm^{-3} s (Sbai and Farida, 2019).

Section S2. Materials

Limonene (>99%, TCI), Δ^3-carene (>97%, Sigma Aldrich), methanol (Optima® LC-MS grade, Fisher Scientific), formic acid (Optima® LC-MS grade, Fisher Scientific), pressured nitrogen gas (99.999%, DEYI) were directly used for nitrogen-blowing without further purification. Ultrapure water with a resistivity of 18.2 MΩ cm was generated with a water purification system (Millipore, France).

Section S3. Calculation of the pure-compound saturation concentrations

The pure-compound saturation concentrations (C_0) of SOA from limonene and Δ^3-carene have been predicted using the following nonlinear expression (Li et al., 2016):

$$\text{Log}_{10}C_0 = \left(n_C^0 - n_C\right)b_C - n_O b_O - 2\frac{n_C n_O}{n_C + n_O}b_{CO}$$

The four free parameters n_C^0, b_C, b_O and b_{CO} represent the carbon number of 1 μg m^{-3} alkane, the carbon-carbon interaction term, the oxygen-oxygen interaction term and the carbon-oxygen nonideality respectively. The two independent variates n_C and n_O are the numbers of carbon and oxygen, respectively. Based on the calculated saturation mass concentration of organic aerosols, they can be classified into five groups (Donahue et al., 2012): extremely low-volatile organic compound (ELVOC; $C_0 < 3\times10^{-4}$ μg m^{-3}); low-volatile organic compound (LVOC; $3\times10^{-4} < C_0 < 0.3$ μg m^{-3}); semi-volatile organic compound (SVOC; $0.3 < C_0 < 300$ μg m^{-3}); intermediate volatility organic compound (IVOC; $300 < C_0 < 3\times10^6$ μg m^{-3}) and volatile organic compounds (VOC; $C_0 > 3\times10^6$ μg m^{-3}).

Table S1. The number and intensity proportion of four groups for limonene

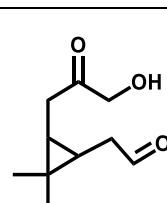| Groups	Monomers	Dimers	Trimers	Tetramers
Number (L)[a]	242	162	122	116
Number (H)[b]	272	187	134	105
Intensity proportion (L)[a]	61.8%	25.7%	9.4%	3.1%
Intensity proportion (H)[b]	65.6%	24.4%	7.9%	2.0%

[a] L means under low RH. [b] H means under high RH.

Table S2. The number and intensity proportion of four groups for Δ^3-carene

Groups	Monomers	Dimers	Trimers	Tetramers
Number (L)[a]	239	178	76	4
Number (H)[b]	216	151	26	1
Intensity proportion (L)[a]	69.8%	28.6%	1.6%	0.5%
Intensity proportion (H)[b]	72.5%	26.9%	2.0%	0.2%

[a] L means under low RH. [b] H means under high RH.
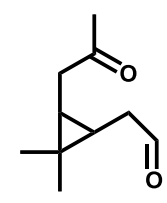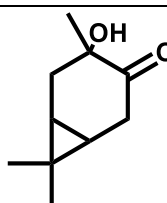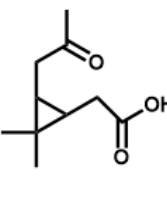
Table S3. Intensity and partitioning coefficient for limonene products identified by MS (can be found in the proposed mechanism).

	Molecular formula	Low RH		High RH		Partitioning coefficient	
		Absolute intensity	Relative intensity	Absolute intensity	Relative intensity	Low RH	High RH
Monomers	$C_{10}H_{16}O_2$	9.01×10^2	1.72×10^{-4}	1.27×10^3	1.42×10^{-4}	0.01	0.02
	$C_9H_{14}O_3$	1.49×10^4	2.85×10^{-3}	3.00×10^4	3.33×10^{-3}	0.02	0.05
	$C_{10}H_{16}O_3$	4.99×10^4	9.54×10^{-3}	8.58×10^4	9.55×10^{-3}	0.05	0.10

	$C_9H_{14}O_4$	1.29×10^5	2.46×10^{-2}	2.46×10^5	2.73×10^{-2}	0.13	0.25
	$C_{10}H_{18}O_3$	1.21×10^3	2.31×10^{-4}	1.64×10^3	1.82×10^{-4}	0.05	0.10
	$C_9H_{16}O_4$	7.60×10^3	1.45×10^{-3}	1.51×10^4	1.68×10^{-3}	0.13	0.25
	$C_{10}H_{16}O_4$	1.28×10^5	2.45×10^{-2}	2.24×10^5	2.49×10^{-2}	0.24	0.41
	$C_9H_{14}O_5$	1.28×10^5	2.45×10^{-2}	2.08×10^5	2.33×10^{-2}	0.58	0.76
	$C_9H_{14}O_3$	1.49×10^4	2.85×10^{-3}	3.00×10^4	-	0.02	0.05
	$C_8H_{12}O_4$	6.71×10^4	1.28×10^{-2}	1.35×10^5	-	0.07	0.15
	$C_{10}H_{18}O_2$	2.62×10^2	5.01×10^{-5}	4.60×10^2	5.12×10^{-5}	0.01	0.02
	$C_9H_{16}O_3$	7.20×10^3	1.38×10^{-3}	1.48×10^4	1.64×10^{-3}	0.02	0.05
	$C_{10}H_{14}O_3$	7.34×10^3	1.40×10^{-3}	1.34×10^4	1.50×10^{-3}	0.05	0.10
	$C_9H_{12}O_4$	3.49×10^4	6.66×10^{-3}	5.94×10^4	6.61×10^{-3}	0.13	0.25
	$C_{10}H_{14}O_5$	4.00×10^4	7.64×10^{-3}	5.44×10^4	6.06×10^{-3}	0.71	0.85
	$C_9H_{12}O_6$	1.25×10^4	2.38×10^{-3}	2.08×10^4	2.31×10^{-3}	0.94	0.97
	$C_{10}H_{16}O_6$	-	8.32×10^{-3}	7.12×10^4	7.93×10^{-3}	0.96	0.98
	$C_{10}H_{18}O_4$	-	1.49×10^{-3}	1.29×10^5	1.44×10^{-3}	0.24	0.41
	$C_9H_{16}O_5$	1.40×10^4	2.67×10^{-3}	2.76×10^4	3.08×10^{-3}	0.58	0.76
	$C_{10}H_{18}O_6$	-	1.39×10^{-3}	1.31×10^5	1.46×10^{-3}	0.96	0.98
	$C_{10}H_{16}O_5$	8.02×10^3	1.53×10^{-2}	1.49×10^4	1.65×10^{-2}	0.72	0.85
	$C_9H_{14}O_6$	-	-	9.40×10^4	1.05×10^{-2}	0.94	0.97
	$C_{10}H_{18}O_5$	9.05×10^3	1.73×10^{-3}	1.65×10^4	1.84×10^{-3}	0.72	0.85
	$C_9H_{16}O_6$	-	-	1.41×10^4	1.57×10^{-3}	0.94	0.97
HOMs	$C_9H_{14}O_7$	-	4.19×10^{-3}	4.44×10^4	4.95×10^{-3}	1.00	1.00
	$C_{10}H_{14}O_7$	8.75×10^3	1.67×10^{-3}	1.32×10^4	1.47×10^{-3}	1.00	1.00
	$C_{10}H_{14}O_{11}$	-	-	3.68×10^2	4.10×10^{-5}	1.00	1.00
	$C_{10}H_{14}O_{13}$	-	-	3.88×10^2	4.32×10^{-5}	1.00	1.00
	$C_9H_{16}O_7$	7.71×10^3	1.47×10^{-3}	1.91×10^4	2.13×10^{-3}	1.00	1.00
	$C_{10}H_{16}O_7$	1.63×10^4	3.12×10^{-3}	3.00×10^4	3.35×10^{-3}	1.00	1.00
	$C_9H_{14}O_8$	-	-	4.12×10^3	4.60×10^{-4}	1.00	1.00
	$C_{10}H_{18}O_7$	4.70×10^3	8.99×10^{-4}	8.90×10^3	9.91×10^{-4}	1.00	1.00

	Formula						
	$C_9H_{16}O_8$	-	-	2.54×10^3	2.82×10^{-4}	1.00	1.00
	$C_{10}H_{16}O_8$	3.63×10^3	6.94×10^{-4}	7.08×10^3	7.67×10^{-4}	1.00	1.00
Dimers	$C_{20}H_{34}O_4$	-		4.98×10^2	5.55×10^{-5}	1.00	1.00
	$C_{18}H_{30}O_6$	-	-	2.74×10^3	3.04×10^{-4}	1.00	1.00
	$C_{18}H_{28}O_7$	-	-	1.53×10^4	1.70×10^{-3}	1.00	1.00
	$C_{20}H_{30}O_8$	3.61×10^2	1.97×10^{-4}	1.25×10^4	1.40×10^{-3}	1.00	1.00
	$C_{18}H_{26}O_8$	1.29×10^4	2.47×10^{-3}	2.34×10^4	2.62×10^{-3}	1.00	1.00

Table S4. Δ^3-carene-SOA identified under high RH in Fig. S3.

[M–H]-	Theo. Mass	Error (ppm)	DBE	Suggested Formula	Molecular Structure
167.10657	167.107753	7.081	3	$C_{10}H_{16}O_2$	
183.101733	183.102668	5.105	3	$C_{10}H_{16}O_3$	
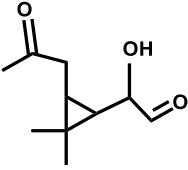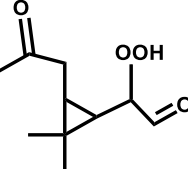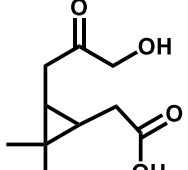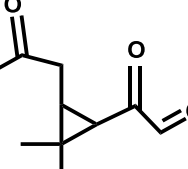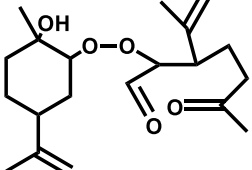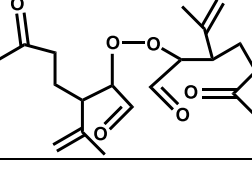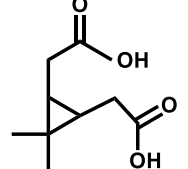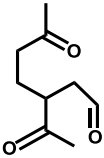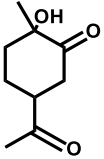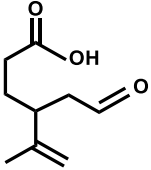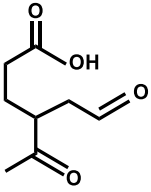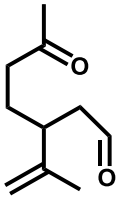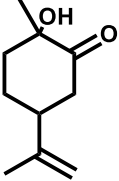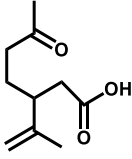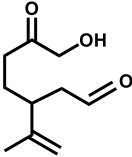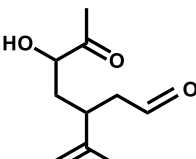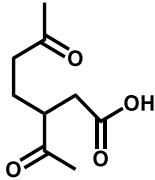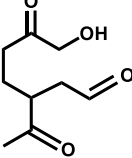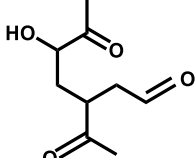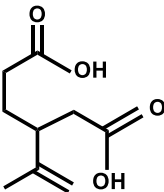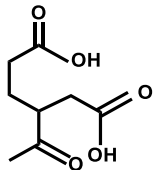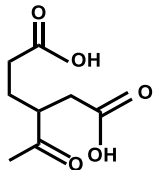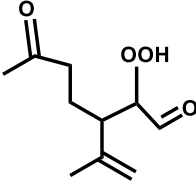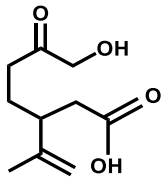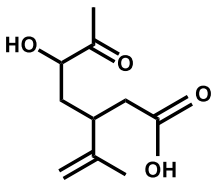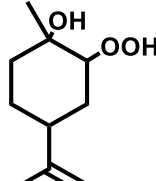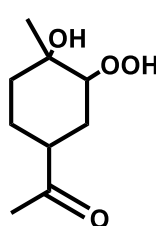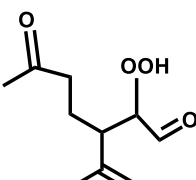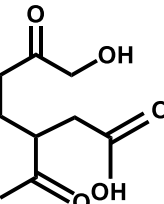
169.122233	169.123403	6.921	2	$C_{10}H_{18}O_2$	
199.096239	199.097583	6.747	3	$C_{10}H_{16}O_4$	
181.085655	181.087018	7.526	3	$C_{10}H_{14}O_3$	
351.214938	351.217698	7.858	5	$C_{20}H_{32}O_5$	
365.194982	365.196962	5.421	6	$C_{20}H_{30}O_6$	
185.080938	185.081932	5.374	3	$C_9H_{14}O_4$	

Table S5. Limonene-SOA under high RH identified in Fig. 3 and Fig. 4.

[M–H]⁻	Theo. Mass	Error (ppm)	DBE	Suggested Formula	Molecular Structure
169.086288	169.087018	4.319	3	$C_9H_{14}O_3$	
183.065329	183.066282	5.208	4	$C_9H_{12}O_4$	
167.107219	167.107753	3.198	2	$C_{10}H_{16}O_2$	

183.102508	183.102668	0.874	3	$C_{10}H_{16}O_3$	
185.081203	185.081932	3.943	3	$C_9H_{14}O_4$	
187.060122	187.061197	5.749	3	$C_8H_{12}O_5$	

199.096857	199.097583	3.644	3	$C_{10}H_{16}O_4$	
185.117126	185.118318	6.441	2	$C_{10}H_{18}O_3$	
187.096428	187.097583	6.172	2	$C_9H_{16}O_4$	
201.075661	201.076847	5.896	3	$C_9H_{14}O_5$	
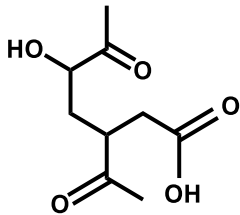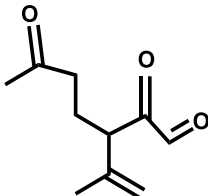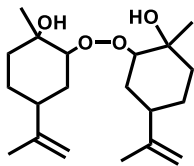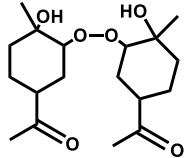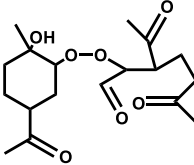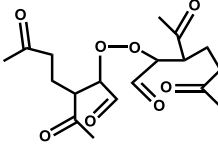
181.086015	181.087018	5.536	4	$C_{10}H_{14}O_3$	
337.237472	337.238433	2.851	4	$C_{20}H_{34}O_4$	
341.196189	341.196962	2.266	4	$C_{18}H_{30}O_6$	
355.17525	355.176227	2.749	5	$C_{18}H_{28}O_7$	
369.154689	369.155491	2.174	6	$C_{18}H_{26}O_8$	

Table S6. The intensity of dimers from multi-carbonyls under high RH and low RH

Molecular formula	Absolute intensity (Low RH)	Relative intensity (Low RH)	Absolute intensity (High RH)	Relative intensity (High RH)
$C_{19}H_{28}O_5$	3.60×10^2	6.87×10^{-5}	9.28×10^3	2.06×10^{-3}
$C_{19}H_{28}O_7$	5.00×10^3	9.50×10^{-4}	2.73×10^4	6.08×10^{-3}

$C_{19}H_{28}O_6$	1.78×10^3	3.40×10^{-4}	1.39×10^4	3.10×10^{-3}
$C_{18}H_{28}O_6$	3.19×10^3	6.08×10^{-4}	4.30×10^3	9.56×10^{-4}
$C_{18}H_{24}O_6$			6.06×10^2	1.35×10^{-4}
$C_{18}H_{26}O_5$			6.28×10^2	1.40×10^{-4}

Table S7. Dimers: RH-dependent discoveries for limonene and Δ^3-carene.

54 dimers exclusively detected under high RH (limonene)		63 dimers exclusively detected under low RH (Δ^3-carene)	
Molecular formula	Absolute intensity (High RH)	Molecular formula	Absolute intensity (Low RH)
$C_{18}H_{26}O_4$	4.66×10^2	$C_{17}H_{24}O_5$	1.59×10^3
$C_{16}H_{20}O_6$	7.24×10^2	$C_{10}H_{14}O_{11}$	3.90×10^3
$C_{13}H_{18}O_9$	3.36×10^2	$C_{14}H_{14}O_8$	4.02×10^3
$C_{17}H_{22}O_6$	6.63×10^3	$C_{20}H_{40}O_2$	4.60×10^3
$C_{18}H_{26}O_5$	6.28×10^2	$C_{12}H_{10}O_{10}$	4.00×10^3
$C_{19}H_{32}O_4$	1.58×10^3	$C_{13}H_{16}O_9$	8.34×10^3
$C_{15}H_{18}O_8$	1.65×10^3	$C_{19}H_{26}O_4$	4.96×10^3
$C_{13}H_{12}O_{10}$	8.85×10^3	$C_{17}H_{22}O_6$	1.05×10^3
$C_{14}H_{20}O_9$	8.44×10^2	$C_{13}H_{12}O_{10}$	5.46×10^3
$C_{16}H_{28}O_7$	9.89×10^3	$C_{13}H_{18}O_{10}$	4.68×10^3
$C_{15}H_{26}O_8$	2.18×10^3	$C_{15}H_{12}O_9$	4.22×10^3
$C_{10}H_8O_{13}$	6.33×10^3	$C_{10}H_{12}O_{13}$	5.00×10^3
$C_{18}H_{24}O_6$	6.06×10^2	$C_{22}H_{28}O_3$	8.88×10^3
$C_{11}H_{14}O_{12}$	7.70×10^2	$C_{19}H_{26}O_6$	1.54×10^3
$C_{21}H_{22}O_4$	4.80×10^3	$C_{16}H_{20}O_9$	1.64×10^3
$C20H34O4$	2.53×10^3	$C_{15}H_{18}O_{10}$	5.00×10^3
$C_{23}H_{32}O_2$	2.12×10^3	$C_{16}H_{22}O_9$	1.69×10^3
$C_{18}H_{32}O_6$	3.68×10^2	$C_{18}H_{22}O_8$	3.32×10^3
$C_{17}H_{30}O_7$	7.46×10^3	$C_{12}H_{16}O_{13}$	4.00×10^3
$C_{14}H_{22}O_{10}$	4.04×10^3	$C_{20}H_{32}O_6$	8.21×10^3
$C_{21}H_{36}O_4$	1.36×10^4	$C_{16}H_{18}O_{10}$	4.50×10^3
$C_{17}H_{30}O_8$	4.68×10^2	$C_{16}H_{20}O_{10}$	5.20×10^3
$C_{12}H_{16}O_{13}$	2.43×10^3	$C_{19}H_{24}O_8$	8.21×10^3
$C_{11}H_{14}O_{14}$	4.46×10^2	$C_{20}H_{28}O_7$	2.38×10^3
$C_{18}H_{30}O_8$	4.46×10^2	$C_{17}H_{20}O_{10}$	4.16×10^3
$C_{16}H_{26}O_{10}$	7.44×10^2	$C_{21}H_{36}O_6$	8.03×10^3
$C_{17}H_{20}O_{10}$	2.12×10^3	$C_{16}H_{26}O_{11}$	1.16×10^3
$C_{16}H_{24}O_{11}$	1.48×10^3	$C_{17}H_{26}O_{11}$	1.32×10^3
$C_{20}H_{24}O_8$	3.96×10^3	$C_{18}H_{18}O_{11}$	4.02×10^3
$C_{17}H_{22}O_{11}$	2.48×10^3	$C_{18}H_{22}O_{11}$	4.54×10^3
$C_{21}H_{34}O_8$	1.28×10^4	$C_{18}H_{26}O_{11}$	1.49×10^3
$C_{13}H_{22}O_{15}$	4.06×10^2	$C_{22}H_{28}O_8$	4.62×10^3

$C_{19}H_{32}O_{10}$	5.30×10^2	$C_{15}H_{18}O_{14}$	4.08×10^3
$C_{22}H_{32}O_8$	5.90×10^3	$C_{20}H_{32}O_{10}$	5.97×10^3
$C_{20}H_{28}O_{10}$	1.53×10^3	$C_{17}H_{22}O_{13}$	5.10×10^3
$C_{18}H_{18}O_{13}$	4.49×10^3	$C_{21}H_{28}O_{10}$	4.25×10^3
$C_{19}H_{24}O_{12}$	1.49×10^4	$C_{19}H_{22}O_{12}$	5.44×10^3
$C_{19}H_{30}O_{12}$	6.10×10^2	$C_{22}H_{34}O_9$	7.52×10^3
$C_{15}H_{18}O_{16}$	1.14×10^3	$C_{21}H_{34}O_{10}$	2.12×10^3
$C_{23}H_{38}O_9$	4.34×10^2	$C_{14}H_{24}O_{16}$	4.80×10^3
$C_{32}H_{44}O_2$	8.96×10^2	$C_{15}H_{22}O_{16}$	4.04×10^3
$C_{21}H_{36}O_{11}$	3.74×10^2	$C_{17}H_{30}O_{14}$	3.51×10^3
$C_{14}H_{26}O_{17}$	1.00×10^3	$C_{22}H_{36}O_{10}$	4.02×10^3
$C_{20}H_{26}O_{13}$	1.26×10^4	$C_{18}H_{24}O_{14}$	4.44×10^3
$C_{22}H_{34}O_{11}$	1.92×10^3	$C_{19}H_{28}O_{13}$	6.68×10^3
$C_{20}H_{30}O_{13}$	9.36×10^2	$C_{20}H_{22}O_{13}$	3.90×10^3
$C_{18}H_{24}O_{15}$	2.05×10^3	$C_{21}H_{26}O_{12}$	4.48×10^3
$C_{21}H_{38}O_{12}$	9.16×10^2	$C_{22}H_{30}O_{11}$	2.29×10^3
$C_{24}H_{38}O_{10}$	3.78×10^3	$C_{15}H_{24}O_{17}$	4.70×10^3
$C_{16}H_{24}O_{17}$	1.26×10^3	$C_{25}H_{38}O_9$	5.24×10^3
$C_{21}H_{24}O_{14}$	4.80×10^3	$C_{17}H_{26}O_{16}$	5.18×10^3
$C_{20}H_{34}O_4$	4.98×10^2	$C_{21}H_{26}O_{13}$	4.82×10^3
$C_{18}H_{30}O_6$	2.74×10^3	$C_{22}H_{30}O_{12}$	2.47×10^3
$C_{18}H_{28}O_7$	1.53×10^4	$C_{16}H_{24}O_{17}$	5.16×10^3
		$C_{17}H_{28}O_{16}$	6.58×10^3
		$C_{29}H_{44}O_6$	5.82×10^3
		$C_{17}H_{30}O_{16}$	2.06×10^3
		$C_{22}H_{38}O_{12}$	3.86×10^3
		$C_{16}H_{32}O_{17}$	7.04×10^3
		$C_{23}H_{30}O_{12}$	1.26×10^3
		$C_{24}H_{34}O_{11}$	6.82×10^3
		$C_{20}H_{30}O_{10}$	4.14×10^3
		$C_{20}H_{32}O_{11}$	3.41×10^3

Table S8. Intensity and partitioning coefficient for Δ^3-carene products identified by MS (can be found in the proposed mechanism).

	Molecular formula	Low RH		High RH		Partitioning coefficient	
		Absolute intensity	Relative intensity	Absolute intensity	Relative intensity	Low RH	High RH
HOMs	$C_{10}H_{14}O_{11}$	3.41×10^2	5.44×10^{-5}	-	-	1.00	1.00

40

	Formula						
	C$_{10}$H$_{16}$O$_8$	1.42×10^3	2.26×10^{-4}	8.31×10^2	1.89×10^{-4}	1.00	1.00
	C$_{10}$H$_{18}$O$_{11}$	2.32×10^3	3.70×10^{-4}	1.61×10^3	3.65×10^{-4}	1.00	1.00
	C$_{10}$H$_{18}$O$_8$	4.60×10^2	7.34×10^{-5}	-	-	1.00	1.00
Dimers	C$_{20}$H$_{30}$O$_6$	1.25×10^4	1.97×10^{-3}	7.55×10^3	1.71×10^{-3}	1.00	1.00
	C$_{20}$H$_{30}$O$_8$	6.99×10^3	1.11×10^{-3}	4.16×10^3	9.44×10^{-4}	1.00	1.00
	C$_{20}$H$_{30}$O$_{10}$	3.62×10^3	5.77×10^{-4}	-	-	1.00	1.00
	C$_{20}$H$_{32}$O$_7$	1.58×10^4	2.51×10^{-3}	7.45×10^3	1.69×10^{-3}	1.00	1.00
	C$_{20}$H$_{32}$O$_9$	1.31×10^4	2.09×10^{-3}	8.76×10^3	1.99×10^{-3}	1.00	1.00
	C$_{20}$H$_{32}$O$_{11}$	2.98×10^3	4.76×10^{-4}	-	-	1.00	1.00
	C$_{20}$H$_{32}$O$_{13}$	5.11×10^2	8.15×10^{-5}	3.12×10^2	7.09×10^{-5}	1.00	1.00

Table S9. The experimental data and results of β-caryophyllene oxidation.

Exp.	[Precursor] (ppb)	[O]$_3$ (ppm)	T (K)	RH (%)	N$_{(14.1-735nm)}$[a] (no.cm^{-3})	M$_{(14.1-735nm)}$[b] (μg m^{-3})	D$_{(mean)}$[c] (nm)	SOA yield (%)
1	234.9	6.3	298	3.2	(2.3±0.1)×10^6	168.2±13.8	49.9±2.5	9.4±0.8
2	255.3	6.4	298	58	(3.6±0.5)×10^6	584.1±10.9	64.3±0.7	25.1±0.5

[a] N$_{(14.1-735\ nm)}$ means the total particle number concentration from size 13.8 nm to 723.4 nm. [b] M$_{(13.8-723.4\ nm)}$ means the total particle mass concentration from size13.8 nm to 723.4 nm. [c] D$_{(mean)}$ means the particle mean diameter.
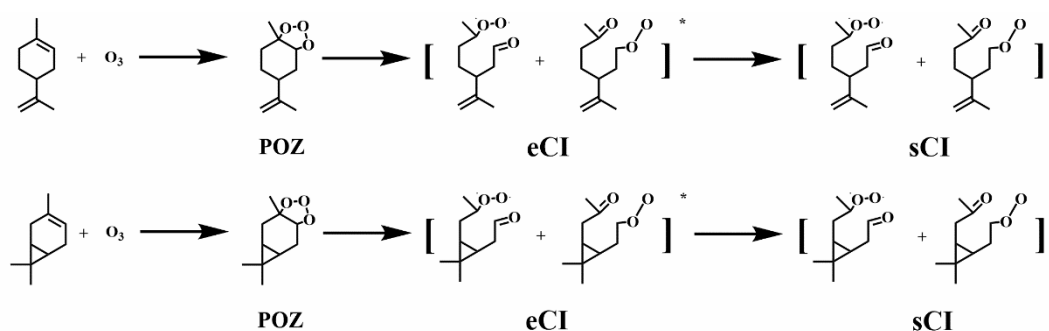

Fig S1. The formation of sCIs from the ozonolysis of limonene and Δ^3-carene.
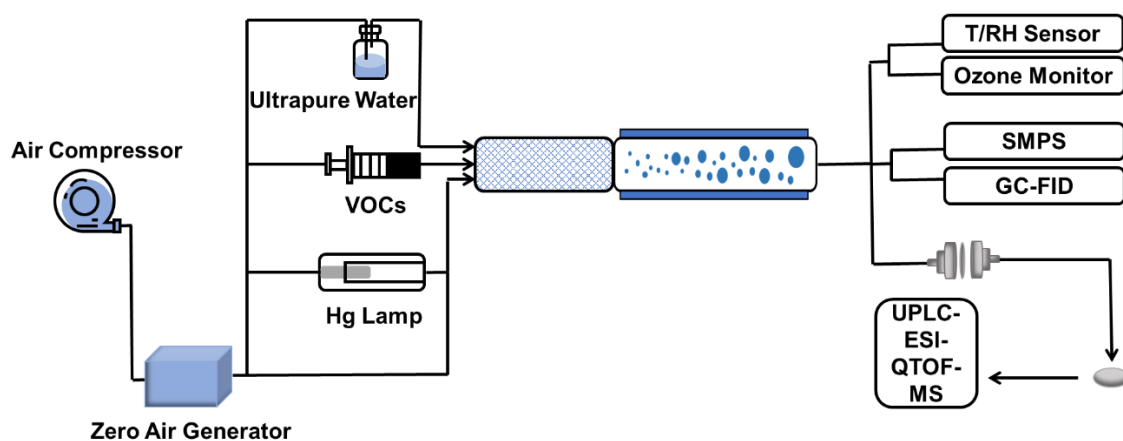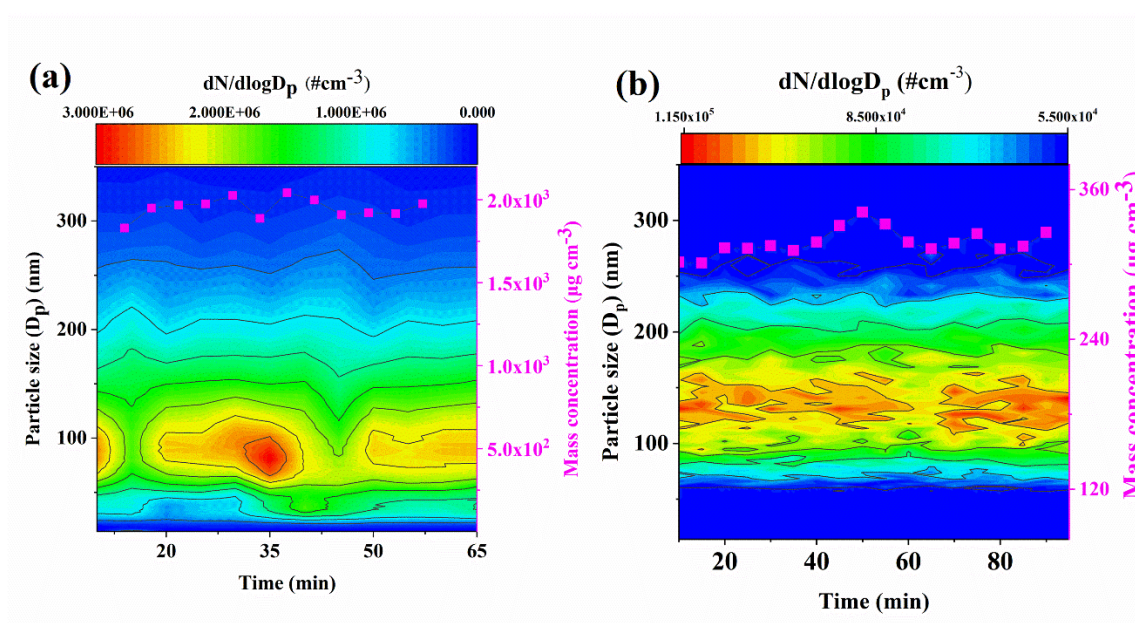
Figure S2. Schematic description of the experiment.

Figure S3. Time evolution of SOA size (electromobility diameter) and mass concentration obtained from limonene/O_3 and Δ^3-carene/O_3 experiments (Exp. 6 and Exp. 11).
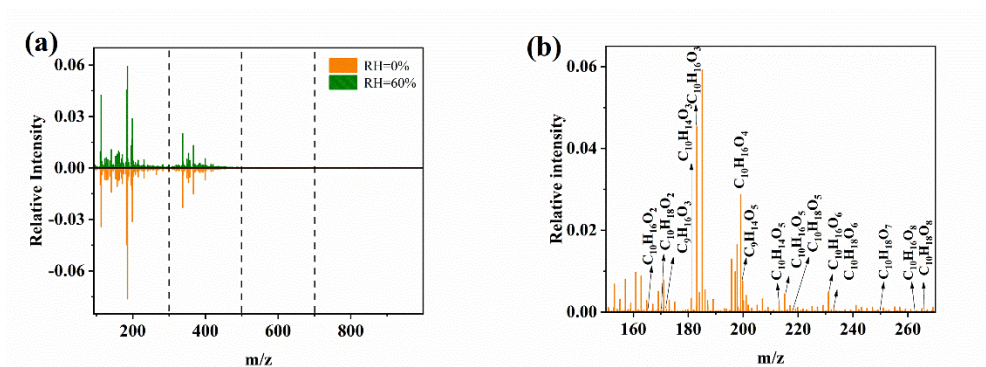
Fig. S4. UPLC/ (−) ESI-Q-TOF-MS mass spectra of SOA from Δ³-carene ozonolysis. (a) MS under high and low RH conditions; (b) the identification of monomers under low RH condition.
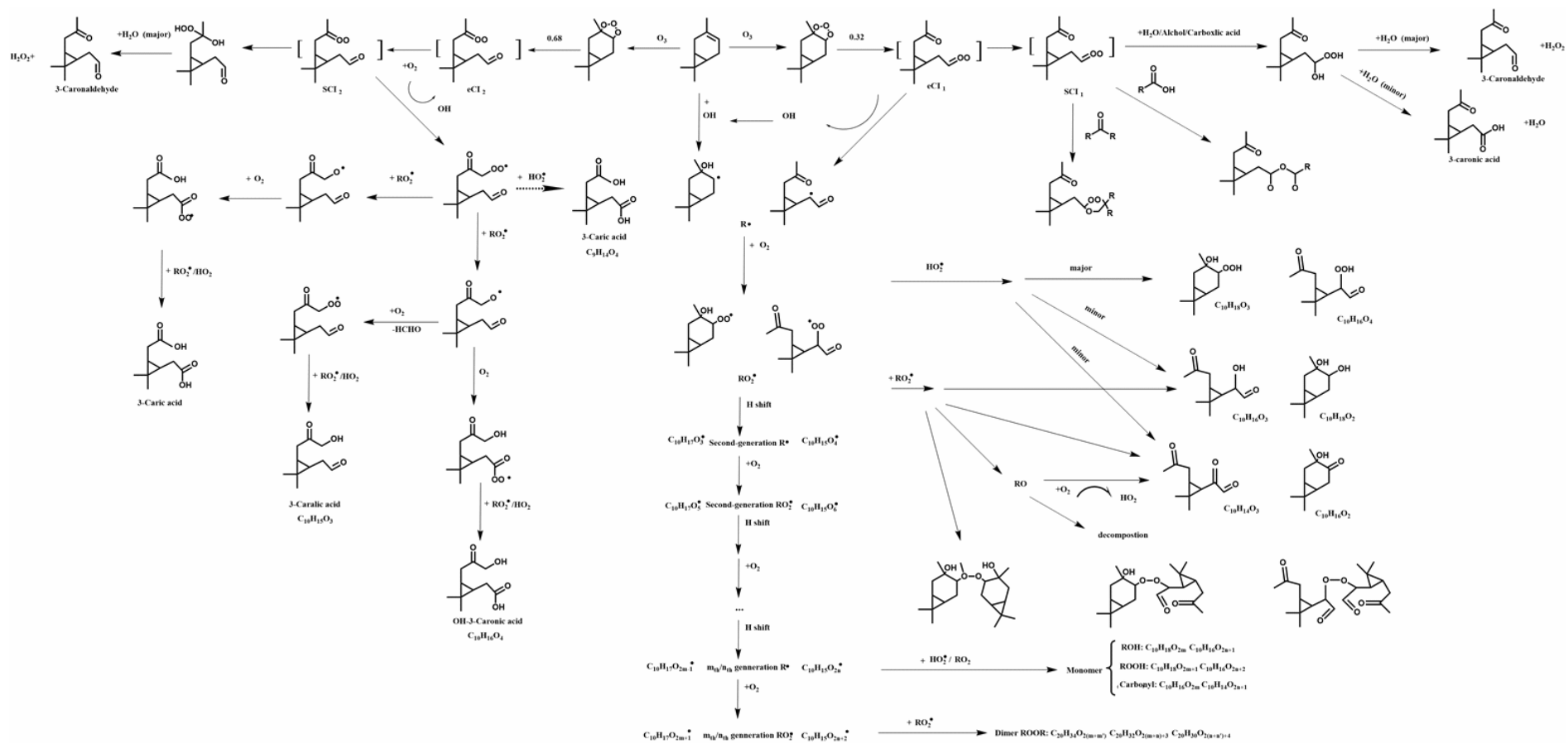
Figure S5. Proposed formation mechanisms for SOA formation from Δ^3-carene ozonolysis under high RH.
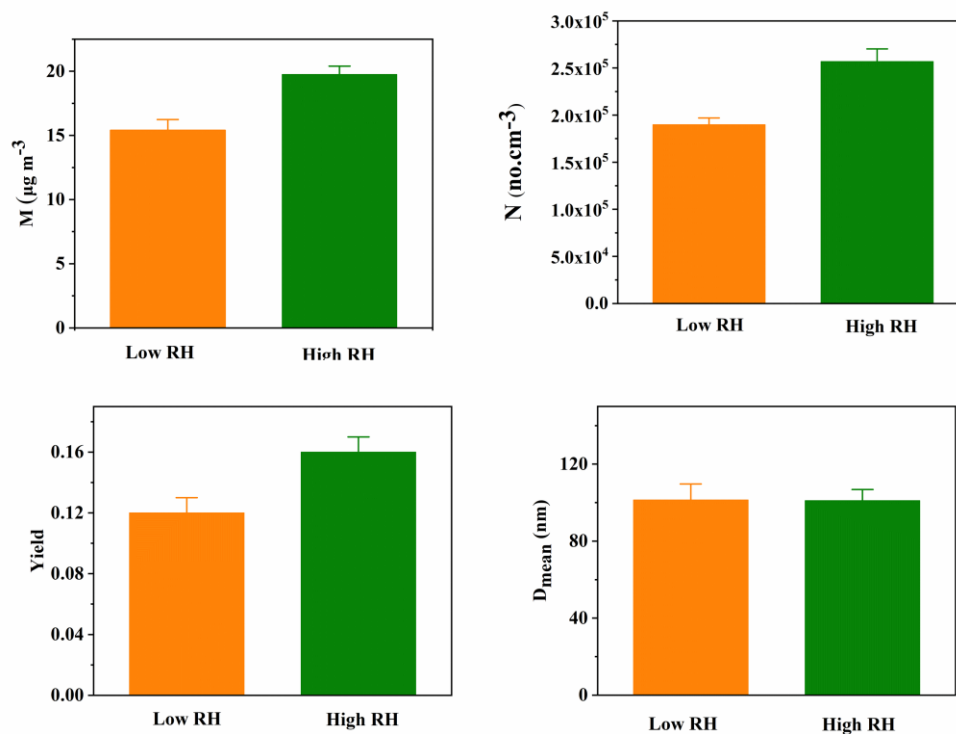
Figure S6. The SOA formation of low-concentration limonene under low and high RH (a) mass concentration (b) number concentration (c) SOA yield (d) mean diameter.
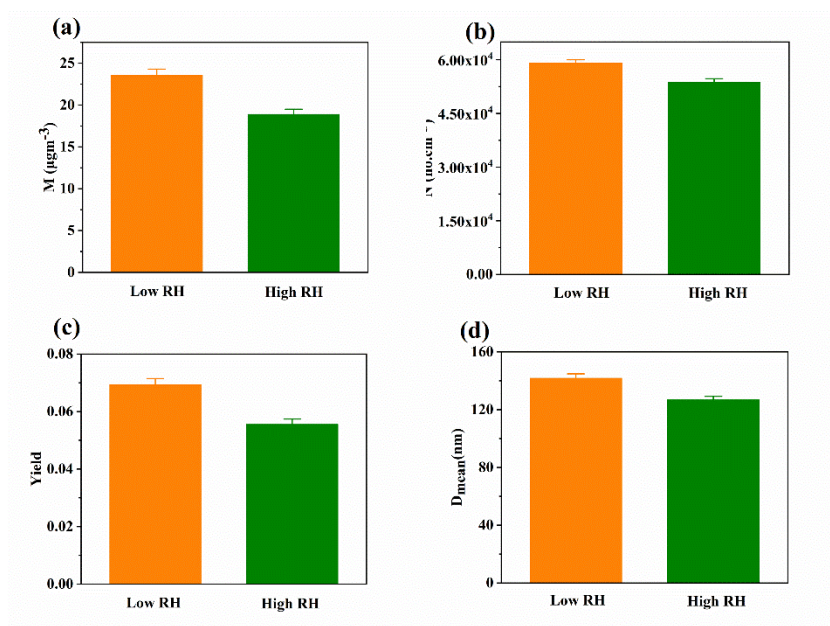

Figure S7. The SOA formation from endocyclic ozonolysis of limonene under low and high RH (a) mass concentration (b) number concentration (c) SOA yield (d) mean diameter. The initial concentration of limonene is 450 ppb and the concentration of O_3 is 67 ppb. Limonene ozonolysis primarily took place on endo-double bonds, with a rate constant of 2.01×10^{-16} cm^3 molec.$^{-1}$ s^{-1} (Shu and Atkinson, 1994).

Based on this rate constant, it can be estimated that approximately 10% of the limonene was consumed by O_3 upon exiting the reactor.
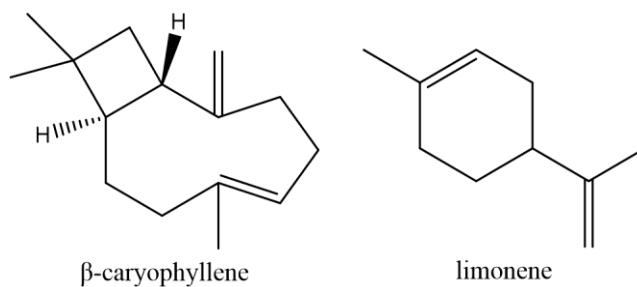

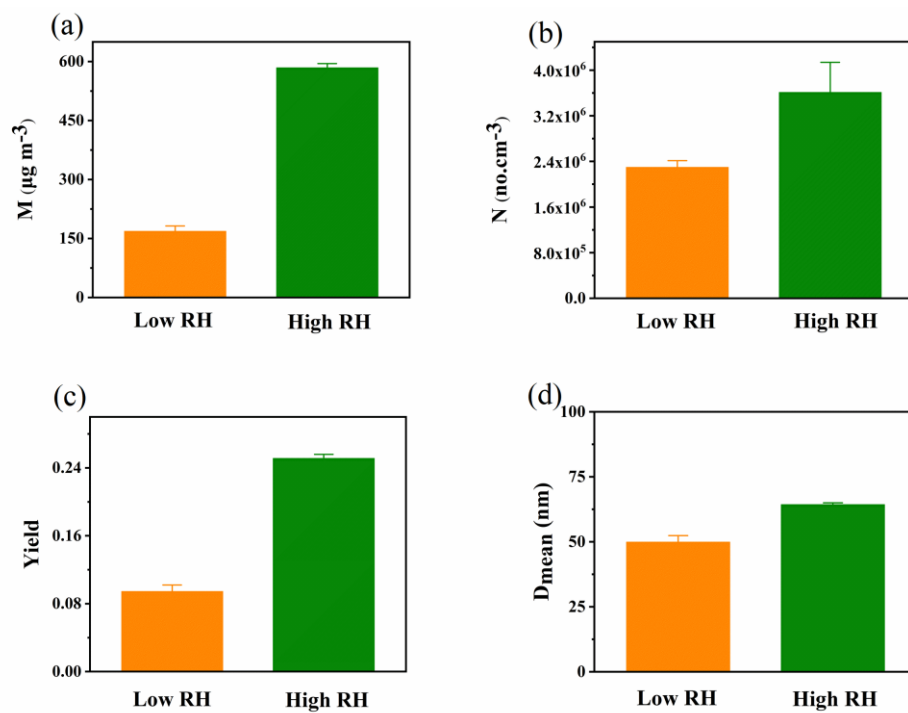**Figure S8.** The molecular structure of β-caryophyllene and limonene.

Figure S9. The SOA formation of β-caryophyllene under low and high RH (a) mass concentration (b) number concentration (c) SOA yield (d) mean diameter.

Reference

Donahue, N. M., Kroll, J. H., Pandis, S. N., and Robinson, A. L.: A two-dimensional volatility basis set - Part 2: Diagnostics of organic-aerosol evolution, Atmos. Chem. Phys., 12, 615-634, https://doi.org/10.5194/acp-12-615-2012, 2012.

Li, Y., Poeschl, U., and Shiraiwa, M.: Molecular corridors and parameterizations of volatility in the chemical evolution of organic aerosols, Atmos. Chem. Phys., 16, 3327-3344, https://doi.org/10.5194/acp-16-3327-2016, 2016.

Sbai, S. E. and Farida, B.: Photochemical aging and secondary organic aerosols generated from limonene in an oxidation flow reactor, Environ. Sci. Pollut. Res., 26, 18411-18420, https://doi.org/10.1007/s11356-019-05012-5, 2019.

Shu, Y. G. and Atkinson, R.: Rate Constants for the gas-pahse reactions of O_3 with a series of terpenes and OH radical formation from the O_3 reactions with sesquiterpenes at 296 ±2K, Int. J. Chem. Kinet., 26, 1193-1205, 10.1002/kin.550261207, 1994.